2018

# Using multiple environmental tracers to investigate the relative role of soil and deep groundwater in stream water generation for a snow-dominated headwater catchment

Isabellah V. von Trapp
*University of Montana, Missoula*

# USING MULTIPLE ENVIRONMENTAL TRACERS TO INVESTIGATE THE RELATIVE ROLE OF SOIL AND DEEP GROUNDWATER IN STREAM WATER GENERATION FOR A SNOW-DOMINATED HEADWATER CATCHMENT

By

ISABELLAH VICTORIA VON TRAPP

Bachelor of Science, Pacific Lutheran University, Tacoma, WA, 2016

Thesis

presented in partial fulfillment of the requirements
for the degree of

Master of Science
in Geosciences

The University of Montana
Missoula, MT

May 2018

Approved by:

Scott Whittenburg, Dean of The Graduate School
Graduate School

Dr. W. Payton Gardner, Committee Chair
Department of Geosciences

Dr. Kelsey Jencso, Committee Co-Chair
Department of Forest Management

Dr. Nancy Hinman, Committee Co-Chair
Department of Geosciences

von Trapp, Isabellah, M.S., Spring 2018 Geosciences

Using multiple environmental tracers to investigate the relative role of soil and deep groundwater in stream water generation for a snow-dominated headwater catchment

Chairperson: W. Payton Gardner

In this study, seasonal fluctuation of environmental tracers in stream flow, soil water, and deep bedrock groundwater were used to constrain the role of deep bedrock groundwater in streamflow generation for a mountainous headwater catchment. Synoptic measurements of stream discharge, $^{222}Rn$, specific conductivity and major ion concentrations were measured throughout the water year over a 5 km reach of Cap Wallace Creek in the Lubrecht Experimental Forest, Montana, U.S.A. with the intention of understanding groundwater – surface water interactions across spatial and temporal scales. Stage measurements were continually recorded at seven stilling well locations along the reach. Discharge measurements and water samples were taken at these sites throughout the winter, spring, summer, and fall of 2017. Shallow soil and groundwater water level and environmental tracer concentrations from contributing hillslopes were also measured. Dissolved $^{222}Rn$ was used to calculate total subsurface discharge. Multi-component mixing models of major ion chemistry and stream discharge were used to constrain end-member discharge to the stream. Mixing model results were compared to landscape characteristics to identify internal catchment controls on the heterogeneity and duration of subsurface discharge. $^{222}Rn$ modeling suggests that streamflow is dominantly generated by subsurface discharge. End-member mixing analysis indicates that streamflow was partitioned between soil water and groundwater end-members. On average, groundwater comprised 38% of streamflow at the outlet but fluctuated between 26% in the spring and 44% in the early summer. Spatial analyses showed elevation and upslope accumulated area (UAA) to be first-order controls on end-member discharge. Groundwater became a more important component to streamflow at higher catchment scales with lower elevations and higher UAA values, suggesting topography-driven flow. Correlations among landscape and end-member discharge were strong across variable states of catchment 'wetness,' indicating that accumulated elevation and catchment area are robust predictors of groundwater discharge across the landscape ($r^2$ = 0.52-0.98). These results have implications for understanding the processes controlling seasonal watershed streamflow response to snowmelt and for predicting headwater response to changing climatic conditions.

# Table of Contents

## Introduction

In the western United States, a large portion of available surface water is derived from mountainous watersheds. In these watersheds, the snowpack represents a significant portion of the annual precipitation budget and supplies large volumes of water to adjacent lowlands during spring melt. Snowpack depth and duration of storage is a function of watershed climatic conditions. Numerous studies predict increased precipitation in the form of rain, and earlier spring melt throughout the western U.S. as a result of climate change (Cayan *et al.*, 2001; Mote *et al.*, 2005; Barnett *et al.*, 2005). Changing snowpack dynamics could have a dramatic effect on annual stream flow, and the hydrologic regime of snow dominated regions (Messerli *et al*., 2004). Deep groundwater represents a potentially significant source of long-term storage in watershed and will play a strong role in mediating watershed response to changing snowpack conditions (Tague & Grant, 2009). Mountainous catchments have inherently complex topography, geology and climatic settings which exert first order controls on the partitioning of subsurface flow between soil, bedrock and groundwater, and control watershed response to climatic forcing. However, little is known about the role deep bedrock groundwater in streamflow generation in upland catchments, the processes and watershed characteristics controlling bedrock contributions and their variability in space and time.

In order to estimate the volume of subsurface discharge during an input event, streamflow is commonly separated into ‘old’ (pre-existing water prior to a storm or melt event) and ‘new’ (water added during a storm or melt event) components. Event water can be separated into overland, soil and groundwater fractions. Mechanisms which produce overland flow include infiltration excess (Horton 1933) and saturation overland flow (Dunne & Black, 1970; Freeze, 1972*a*). Subsurface storm flow includes saturated soil flow (Hewlett & Hibbert, 1967; Kienzler

& Naef, 2008), and groundwater discharge (Pinder & Jones, 1969; Fritz *et al.*, 1974). Pre-event water is generally derived from subsurface sources including soil flow and groundwater (Sklash *et al.* 1976).

The amount of old water and event water discharging the hydrograph is still a fundamental question in watershed hydrology. The primary method for estimating pre-event and event water is chemical hydrograph separation. Sklash *et al.* (1976) utilized oxygen-18 signatures of rainfall, runoff, and groundwater to separate stream water into its relative components at the source and showed that a significant portion of the storm flow hydrograph is composed of pre-event water. Sklash *et al.* (1976) hypothesized that this large pre-event fraction can be attributed to rapid, near-stream groundwater head gradient increases and resulting rapid increase in groundwater discharge is due to a 'capillary-fringe mechanism.'

Stable isotope-based, two component hydrograph separation has been used to further demonstrate that 'pre-event water' significantly contributes to streamflow during storm or meltwater events (e.g. Sklash & Farvolden, 1979; Herrmann & Stichler, 1980; Hooper & Shoemaker, 1986). Stable isotope separation can be further refined to investigate the source of pre-event water. In watersheds underlain by impermeable bedrock, soil water can be the primary pre-event, subsurface component of streamflow (Kennedy *et al.*,1986). DeWalle *et al.* (1988) utilized a three-component $^{18}O$ tracer model to further partition 'old' (stored) water, into soil water and groundwater components, respectively and found groundwater to account for the majority of streamflow during storms (75-90%), but found soil water to contribute significantly (6-24%) depending largely on antecedent soil moisture conditions. The role of soil water in storm runoff has been further demonstrated as an important contributor to streamflow by numerous other studies (e.g. Swistock *et al.*, 1989; McDonnell *et al.*, 1991).

Separating groundwater and soil water with stable isotopes alone can be problematic. Stable isotope composition may not vary greatly between soil and groundwater (Kennedy et al 1986, Klaus & McDonnell 2013). McDonnell *et al.* (1991) show that deuterium concentrations in groundwater can shift significantly in time *and space* and application can be problematic in steep, humid catchments. Genereux *et al.* (1993) indicate that $^{18}O$ and $^{2}H$ are only useful during stormflow events and hydrograph separation may not be practical if the difference in isotopic composition between the 'old' and 'new' water is not large compared to analytical uncertainty and natural variability in contributing waters.

Major ions provide another dataset to perform chemical hydrograph separations. Hooper *et al.* (1990) applied an End-Member Mixing Analysis approach (EMMA) by plotting solute concentrations of various samples of stream, soil, and groundwater and identifying end member chemical compositions. Stream water was shown to be a mixture of water from various subsurface sources including: the organic horizon layer, the hillslope mineral horizon, and the floodplain mineral horizon. Christophersen (1990) utilized a similar approach but was not able to adequately explain stream water chemistry given various observed soil water end-member concentrations. Genereux *et al.* (1993) note that EMMA is advantageous for separating relative components of streamflow during baseflow and storm flow, but the technique becomes disadvantageous when trying to understand how water moves sequentially from one subsurface zone to another (i.e. infiltration of hillslope water into groundwater) as these types of analyses do not provide information on the rate of chemical signature acquisition from a particular zone.

Other environmental tracers have been utilized to characterize hydrologic flow paths. Radon-222 ($^{222}Rn$), is a sensitive tracer for detecting subsurface discharge in surficial water bodies. $^{222}Rn$ has been used to pinpoint areas of groundwater inflow from mountainous streams in the

Wasatch Mountains, Utah (Rogers, 1958). By combining $^{222}$Rn measurements with a mass balance equation, the volume of groundwater input can be quantified (Lee and Hollyday, 1987; Ellins *et al.*, 1990). Different subsurface zones can have markedly different $^{222}$Rn concentrations, which can elucidate subsurface flow paths and sources (Genereux, 1990). Genereux *et al.* (1993), for example, used the different $^{222}$Rn signatures of vadose zone water, soil water, and bedrock groundwater in a three end-member mixing model and showed groundwater and soil water to be the dominant sources of streamflow during low flows. Kienzler & Naef (2007) used $^{222}$Rn signatures of stream to evaluate the role of pre-event water in subsurface stormflow and found that the formation and fraction of pre-event water contained in SSF is largely dependent on the initiating source. While several studies have used $^{222}$Rn as a tool to learn about groundwater-stream water interactions at small scales (Kies *et al.*, 2005; Kienzler & Naef, 2007), to our knowledge no study has used $^{222}$Rn to quantify subsurface discharge to streamflow across spatial and temporal scales in mountainous, snow-dominated catchments.

Several studies have attempted to understand what watershed features and processes account for spatial heterogeneities and duration of subsurface contribution to streamflow. Catchment area, topography, bedrock permeability and climate have all been postulated as potential mechanisms that control subsurface flow. Grayson *et al.* (1997) compared two catchments to describe two preferred states of soil moisture in which 'wet' and 'dry' states are associated with lateral flow and vertical moisture fluxes, respectively. The study attributed climate and topography as the dominant controls on soil moisture but never addressed how internal variability in catchment topography affected soil moisture patterns across the catchment. McGuire *et al*. (2005) utilized stable isotope signatures of rainfall and runoff to test the idea that the mean water residence time is related to upslope accumulated area. No relationship between

catchment area and residence time was found ($r^2 < 0.01$); however, strong relationships were found between residence time and flow path distance and gradient to the stream network implying that topography exerts a strong influence on water transit time. Jencso *et al.* (2009) utilized hydrometric data from recording wells to test the relationship between increasing catchment scale and runoff dynamics. The study found strong relationships among the duration of hillslope riparian-stream connectivity and upslope accumulated area as well as topography and topology.

Frisbee *et al.* (2011) conducted an experiment to test two hypotheses about streamflow generation in a large (1600 $km^2$) Rocky Mountain alpine catchment. Chemical signatures indicated that the role of groundwater becomes increasingly important at larger watershed scales, suggesting that streamflow is not just the aggregation of individual hillslopes, and that groundwater influence increases with increasing catchment scale. Hale & McDonnell (2016) and Pfister *et al.* (2017) found bedrock permeability to the dominant control on mean transit time of subsurface discharge by observing streamflow in a nested-catchment approach across variable lithologies.

While all of these studies have helped to shed light on the source, mechanism, and duration of subsurface discharge to streamflow, the role of groundwater in snowmelt-dominated catchments still remains elusive. In addition, it is still not well understood how internal structural variability within the catchment controls heterogeneity and duration of subsurface discharge. In this study, we aim to answer the following questions:

Q1: *What are the dominant sources of subsurface contribution to streamflow and how do they change spatially and temporally?*

Q2: *What are the dominant watershed structural features that control the source and distribution of subsurface contribution to streamflow?*

We hypothesize:

H1) *Deep bedrock groundwater is an important source of stream flow generation in Cap Wallace, and that the relative importance of bedrock groundwater changes seasonally.*

H2) *The role of groundwater becomes more important along the reach with increased upslope accumulated area.*

To test these hypotheses, a combination of synoptic $^{222}$Rn, conservative ion, and discharge measurements are used to model end-member discharge ratios across spatial and temporal scales in a small, snowmelt-dominated headwater catchment. The catchment was then 'de-aggregated' into seven sub-catchments where modeled end-member discharges were compared at each of gauging stations along the reach against various terrain characteristics to understand internal catchment variability and its relationship to runoff dynamics.

## Study Area

### *2.1 Location and Geologic Description*

The study area is the Cap Wallace Watershed (CWW) of the Lubrecht Experimental Forest (LEF) in west-central Montana. The LEF is located approximately 56 kilometers northeast of Missoula, Montana on the north slope of the Garnet Range (**figure 1**). The Garnet Range is part of the Northern Rocky Mountains formed by folding and thrusting associated with the Sevier and Laramide Orogenies (140-55 Ma). Extensional normal faulting initiated in the Early Eocene as a result of Basin and Range tectonics, triggering the uplift of metamorphic core complexes in the

Northern Rockies (Portner *et al.,* 2011). CWW sits on the flank of a large granitic batholith called the Garnet Stock which intruded the area during the Late Cretaceous (Lonn *et al*., 2010).

The catchment drains 6 $km^2$ of forested land and is a tributary to Elk Creek and the Blackfoot River. Cap Wallace Creek (CWC) follows an east-west trending normal fault. Quaternary glacial and alluvial deposits cover the narrow valley bottom and stream floor. Hillslopes are composed of gravelly silt loam soils (USDA, 1995) that overlay several kilometers of the Precambrian-aged metasedimentary Belt Supergroup. Once sedimentary fill in a large intracratonic basin, the Belt Formations present in the area have metamorphosed into siltites, argillites, and quartzites. The north-aspect slope is comprised of the Garnet Range Formation, a siltstone with hummocky sand lenses which sits unconformably across the valley from the stratigraphically lower Bonner Quartzite, a massive slightly metamorphosed arkosic sandstone that makes up the south-aspect slopes. Over time, the underlying formations have been subject to tectonism associated with compression from major mountain building events, and subsequent active extension due to gravitational relaxation, leading to a dense fracture network within the bedrock (Brenner, 1968). Fracture networks are likely pathways for groundwater contributing to streamflow (Briar, 1996).

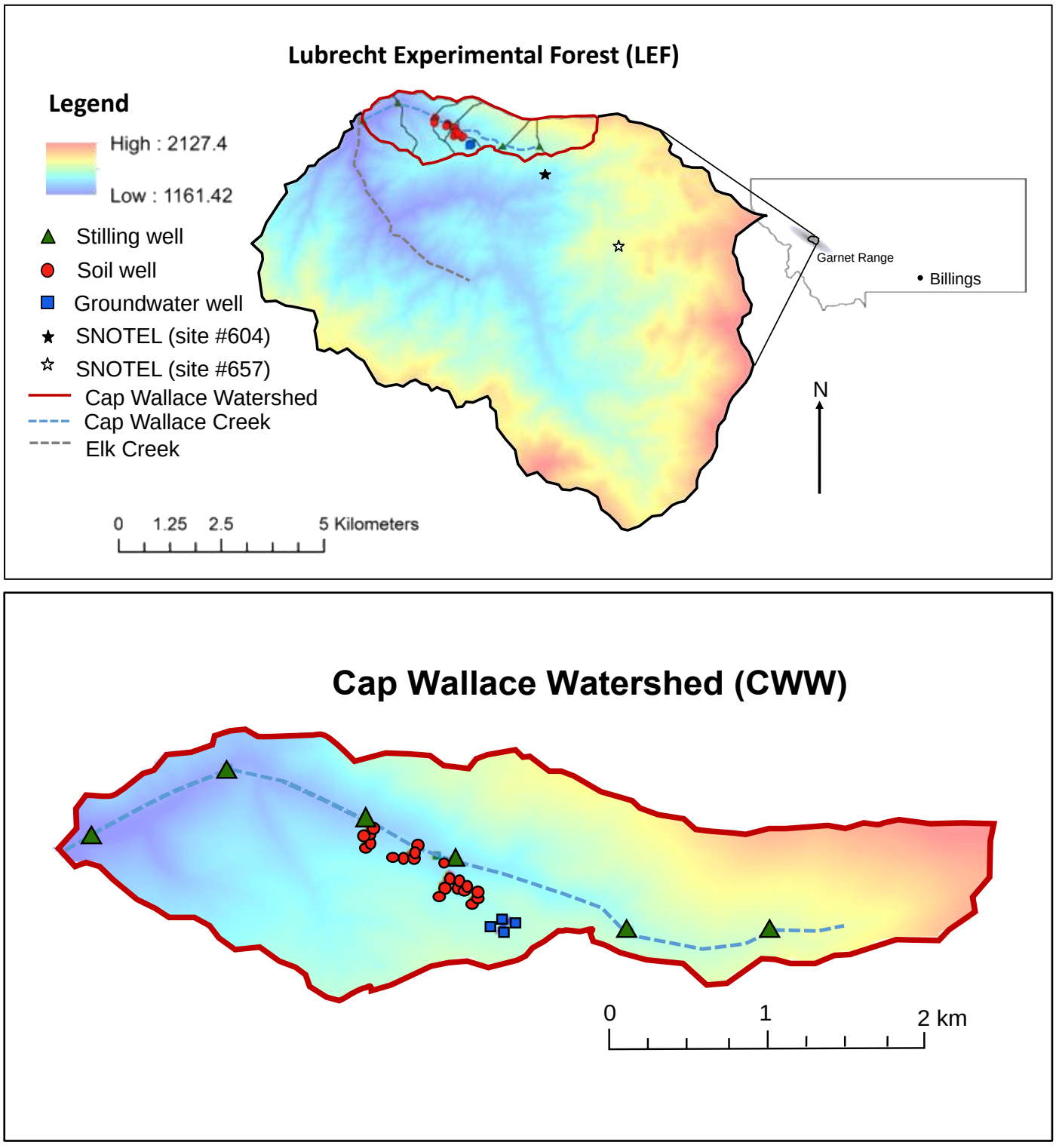


*Figure 1. A regional map of Lubrecht Experimental Forest (LEF) showing its relative location on the north slope of the Garnet Range in west-central Montana. Outlined in red, Cap Wallace Watershed (CWW) was the primary area of focus in this study.*

### *2.2 Climate and Landscape Description*

The Cap Wallace watershed ranges in elevation from 1,163 meters at the confluence of Cap Wallace Creek and Elk Creek, to 1,918 meters at the ridge tops. Vegetation consists primarily of second-growth Western larch (*Larix occidentalis*) on the north slope mid and upper elevations, Douglas-fir (*Pseudotsuga menziesii*) on north facing, low elevation slopes and Ponderosa Pine (*Pinus ponderosa*) on south aspect slopes. North and south aspect slopes differ largely in terms of landscape. North aspect slopes are overlain by well-developed soils, while south aspect slopes have little-to-no soil coverage and are generally covered by steep talus fields. Due to topographic variation in the radiation balance and resulting microclimatic effects (Thornthwaite, 1961; Holden 2011, 2011a), the south aspect slope is much drier throughout the year (Hoylman *et al*., in review).

Using data from the Lubrecht Flume SNOTEL station (site #604; 1425.5 meters), an average yearly precipitation of 514 mm was calculated using data from the last ten years. Nearly fifty percent of precipitation falls as snow, classifying CWW as a snowmelt dominated watershed (Clark, 2015). In 2017, temperatures ranged from -27.6°C to 34.2°C with an annual average of 6.11°C. **Figure 2** shows the daily climatic conditions for the 2017 water year.

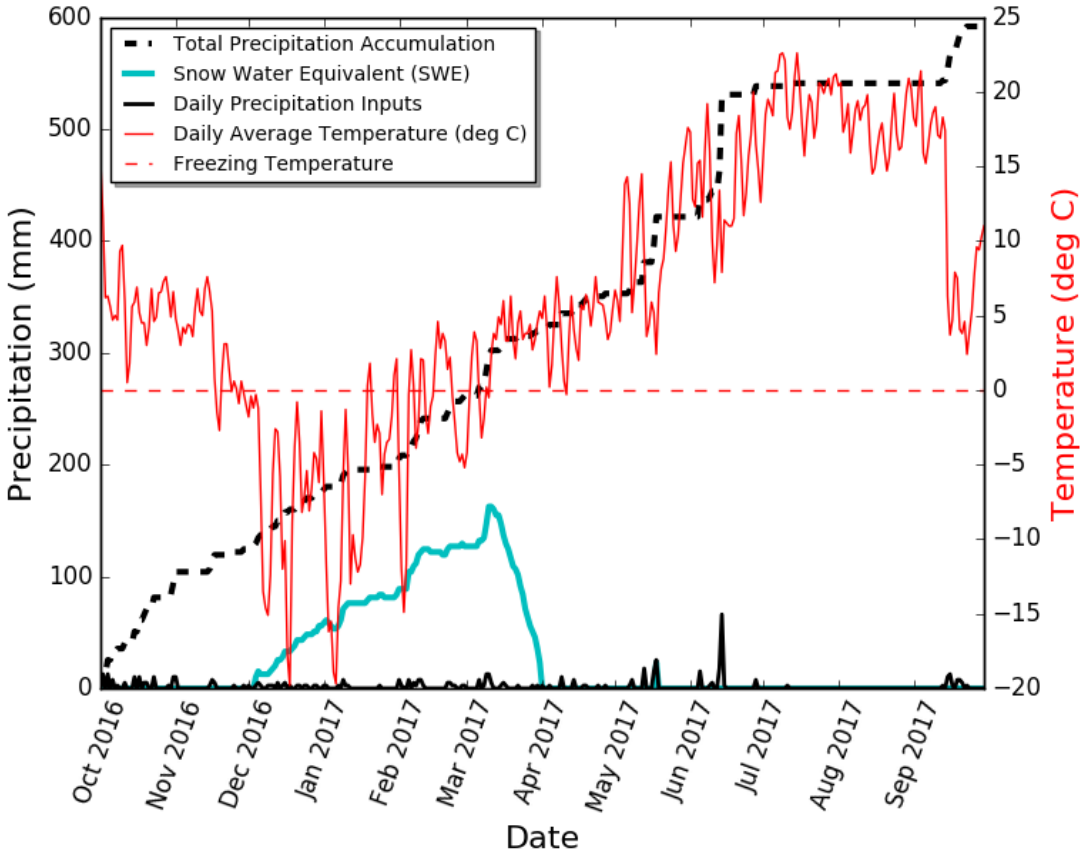


*Figure 2. Lubrecht climate data for the 2017 water year. Data source: Lubrecht SNOTEL (site #604). 2017 was a heavy precipitation year with many days below freezing.*

## 3. Methods

### *3.1 Field Methods*

The catchment is instrumented with 36 shallow soil wells, 4 groundwater wells, and 7 stilling wells for measuring stream discharge, that are strategically located to monitor hydrologic hillslope response both spatially and temporally (**figure 1**). Field work began in LEF during the winter of 2017. Pressure transducers were installed in the stilling, soil, and groundwater wells to continually monitor and record stage measurements along the stream and throughout contributing hillslopes. Throughout the spring, summer, and fall of 2017, synoptic discharge measurements were made repeatedly at each stilling well location across variable flow states. Following the method of Moore (2005), discharge measurements were made by injecting a

known mass of conservative chemical tracer (NaCl) into the stream and solving a simple mass balance equation rearranged to solve for discharge:

$$Q = \frac{M}{\int_0^t C(t)dt} \quad (1)$$

where $Q$ is discharge ($L^3/T$), $M$ is the injected mass (M), and $C$ is the concentration ($M/L^3$) of tracer at time *t* (T). During discharge measurements, an electric conductivity probe was placed downstream of the injected salt 'slug' to capture the change in stream concentration over time. Conductivity was logged every two seconds to measure a break-through curve. Concentration was calculated from conductivity assuming:

$$C\left(\frac{mg}{l}\right) = 0.47 \cdot SC\left(\frac{\mu}{cm}\right) \quad (2)$$

Break-through curves were then numerically integrated and equation (1) used to solve for discharge. Replicate measurements were taken at multiple stilling well locations during our sampling period. On average, replicates were within ± 4% of one another but during baseflow, one replicate measurement recorded a discharge 54% lower than the original measurement (08/28/2017). Low flows have been shown to complicate the dilution gauging technique if hyporheic exchange occurs (Moore, 2004). For that reason, the baseflow measurement was not used to calculate average uncertainty in replicate measurements.

During synoptic discharge measurement campaigns, Cap Wallace Creek was sampled for environmental tracers. Stream water samples were collected for $^{222}Rn$ and major ions. Sample bottles were rinsed three times with sample water. Samples collected for $^{222}Rn$ analysis were collected underwater in airtight glass bottles to avoid exchange with the atmosphere. Major ion samples were collected and sealed in acid washed polyethylene bottles. Field parameters: pH, temperature, oxidation reduction potential, and electric conductivity were collected using an In-

Situ AquaTroll 600 sonde. Water samples were collected from soil and groundwater wells in April of 2017 for environmental tracer content using a peristaltic pump. Prior to collection, wells were purged until field parameters remained constant (~2-3x the volume of the well). Field parameters were collected using a flow through cell. $^{222}$Rn samples were filled with the pump and capped underwater in a bucket containing enough sample water to fully submerge the bottle. Major ions samples were collected after rinsing the bottle three times.

Saturated hydraulic conductivity ($K_{sat}$) measurements of soil wells were made using a constant head permeameter. The constant head permeameter maintains constant water height in bottom of an augured hole situated in the vadose zone, while supplying the hole with water. Infiltration rates were monitored until steady-state flow is reached. Hydraulic conductivity values were then calculated using the Glover method detailed in Amoozegar (1989). Hydraulic conductivity of the deep bedrock system was estimated via slug tests in the groundwater wells. Slug tests were conducted by quickly injecting a volume of water into groundwater wells to cause a rapid rise in hydraulic head. Water level was then recorded over time with a transducer as it fell back to background conditions. Conductivity was estimated from the normalized head relaxation using the Hvorslev (1951) method.

### *3.2 Lab Methods*

Because of its short half-life of 3.8 days, $^{222}$Rn samples were analyzed within 48 hours of collection. Samples were analyzed using a spectral alpha-decay detector – RAD7 Durridge Instruments. $^{222}$Rn concentrations were corrected to account for decay during the period between sample collection and analysis using:

$$C_{tc} = C_i e^{\left(\frac{t}{132.4}\right)} \quad (3)$$

where $C_{tc}$ is the time-corrected radon concentration in (Bq/L), $C_i$ is the initial radon concentration prior to correction (Bq/L), and *t* is the elapsed time between collection and analysis in hours. Samples collected for ion chromatography (IC) and inductively coupled plasma optical emission spectroscopy (ICAP-OES) analyses were filtered using a 0.45 μm disposable filter. Cation samples were acidified with 0.2 mL of nitric acid. Anions were run on the DIONEX DX500 (IC) and cations were analyzed on a Perkin-Elmer OPTIMA 5300 (ICAP-OES). Detection limits and accuracy for IC and ICAP-OES analysis are located in **table 1**. All $^{222}$Rn and major ion samples were analyzed at the University of Montana's Environmental Biogeochemical Laboratory.

*Table 1. Limits of detection and precision of field and lab duplicates for ion chromatography (IC) and inductively coupled plasma emission spectroscopy (ICAP-OES) analyses. Error associated with field and lab duplicates are within an acceptable range for geochemical interpretation.*

| | ***Ca*** | ***K*** | ***Mg*** | ***Na*** | ***F*** | ***Cl*** | ***$SO_4$*** | ***$NO_3$*** |
|---|---|---|---|---|---|---|---|---|
| ***Limit of Detection (mg/L)*** | 0.102 | 0.51 | 0.102 | 0.51 | 0.015 | 0.100 | 0.100 | 0.100 |
| ***Error % (lab)*** | ± 1.35 | ± 1.40 | ± 1.20 | ± 1.12 | ±3.86 | ±2.31 | ±1.78 | ±0.21 |
| ***Error % (field)*** | ± 3.20 | ± 1.80 | ± 3.90 | ± 3.30 | ±6.57 | ±1.86 | ±0.19 | ±5.14 |

### *3.3 Modeling Approach and Data Analysis*

Distinctive chemical signatures amongst the various stream flow sources were used to perform chemical hydrograph separations and infer streamflow sources. Several tracers and analytical techniques were combined and the resulting conceptual model created by comparing and synthesizing the outputs of the different models. **Figure 3** outlines the conceptual framework for the modeling approach. Two different modeling techniques were used to identify end-member contribution to streamflow. Radon was used to calculate total subsurface discharge. End-member mixing analysis (EMMA) was then conducted on the conservative chemical signatures of stream and end-member chemistry to provide a quantitative, non-biased method of

choosing end-members. EMMA derived end-members were then used in a mass-balance mixing model to estimate mixing fractions. Results from each method were compared and synthesized at each stilling well location and the relationship with landscape topographic characteristics investigated. Finally, the effect of different internal landscape characteristics on spatial heterogeneity and duration of subsurface flow at a variety spatial and temporal scales was quantified.

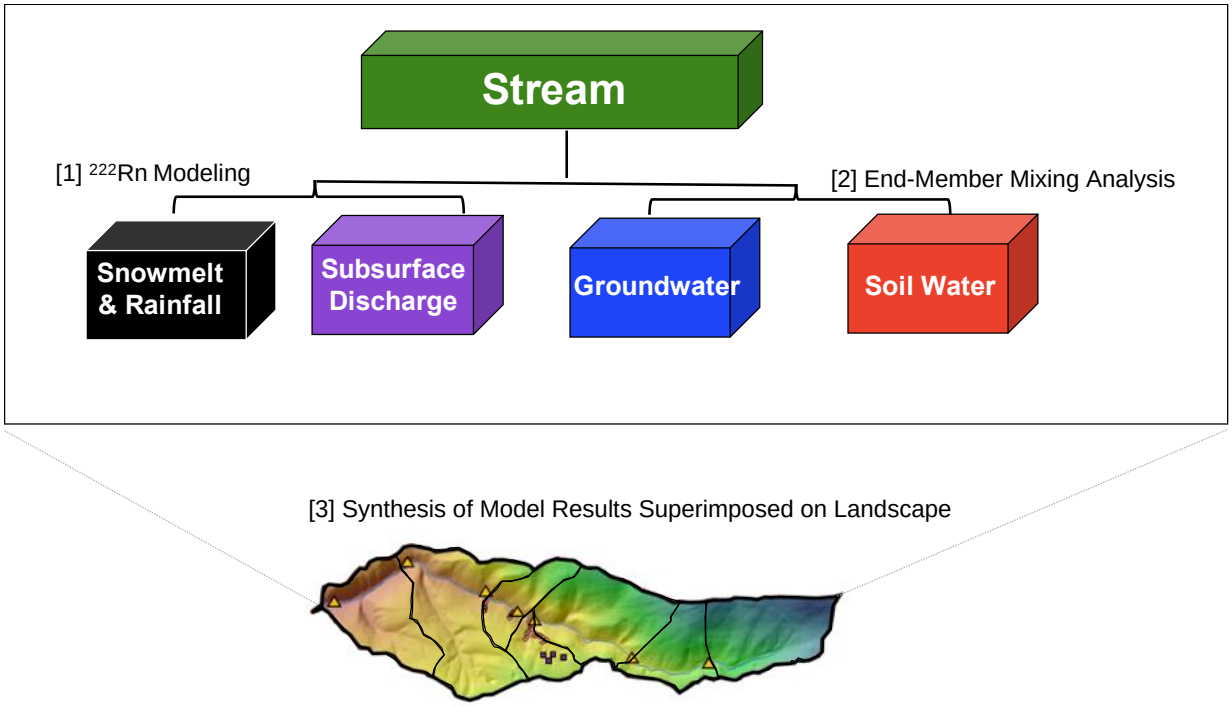


*Figure 3. The step-by-step conceptual framework by which modeling was conducted and spatial analyses were performed.*

### *3.3.1 Radon Modeling*

Common conservative tracers classically used in separation studies (i.e. chloride, $^{18}O$) are present in every reservoir contributing to streamflow including: snowmelt, precipitation, overland, soil and groundwater. $^{222}Rn$ is advantageous because it is not present in the atmosphere and therefore non-existent in meteoric water (overland, snowmelt and precipitation). Thus, $^{222}Rn$ concentrations can be used to isolate subsurface stream flow sources. In addition, separating streamflow into its relative components becomes problematic when tracer concentrations shift in

time and space. Ionic concentrations of groundwater are a function of flow velocity, residence time, rate of kinetic mineral weathering, and available surface area of weatherable material (Goldich, 1938). As such, groundwater chemical signatures can evolve with longer residence times which can be challenging when applying average end-member chemical concentrations to mixing models. $^{222}$Rn reaches secular equilibrium after two weeks in the subsurface, thus the subsurface in most cases can be assumed to be at steady state.

Traditional mass balance mixing equations, derived for conservative tracers cannot be used for radioactive, gas-phase tracers. Instead, estimating subsurface inflow from $^{222}$Rn requires a model that accounts for subsurface discharge, gas exchange with the atmosphere, and radioactive decay (**figure 4**). A 1D stream transport model was created to simulate longitudinal radon activity after Cook *et al.* (2006) using equations:

$$\frac{\partial Q}{\partial x} = I(x) - L(x) - E(x) \tag{4}$$

$$Q\frac{\partial c}{\partial x} = I(c_i - c) + wEc - kwc - dw\lambda c \tag{5}$$

where $c$ is the concentration of radon in the stream (Bq/L), $c_i$ is the concentration of radon in groundwater or soil water (Bq/L), $I$ is the groundwater inflow rate (m$^3$/m/day), $w$ is the stream width (m), $d$ is the mean stream depth (cross-sectional area/width) (m), $k$ is the gas exchange velocity (m/day), $\lambda$ is the radon decay coefficient (per day), $Q$ is the stream discharge (m$^3$/day), $E$ is the evaporation rate (m/day), and $L$ is the stream extraction rate (m$^3$/m/day). Equation 4 is the mass balance equation for discharge in the stream, and Equation 5 is the 1D, steady-state equation for solute transport in the stream.

The model assumes zero atmospheric concentration, no production of $^{222}$Rn within the stream, and steady state flow conditions (Cook *et al.*, 2006). Distributed groundwater discharge

was estimated using a least-squares fit of modeled and observed $^{222}$Rn by varying the groundwater discharge step function after Gardner (2011). For each sampling period, total subsurface discharge including soil water and groundwater were lumped into one term. Total subsurface discharge was then used to estimate snowmelt discharge under the assumption that snowmelt has zero radon concentration.

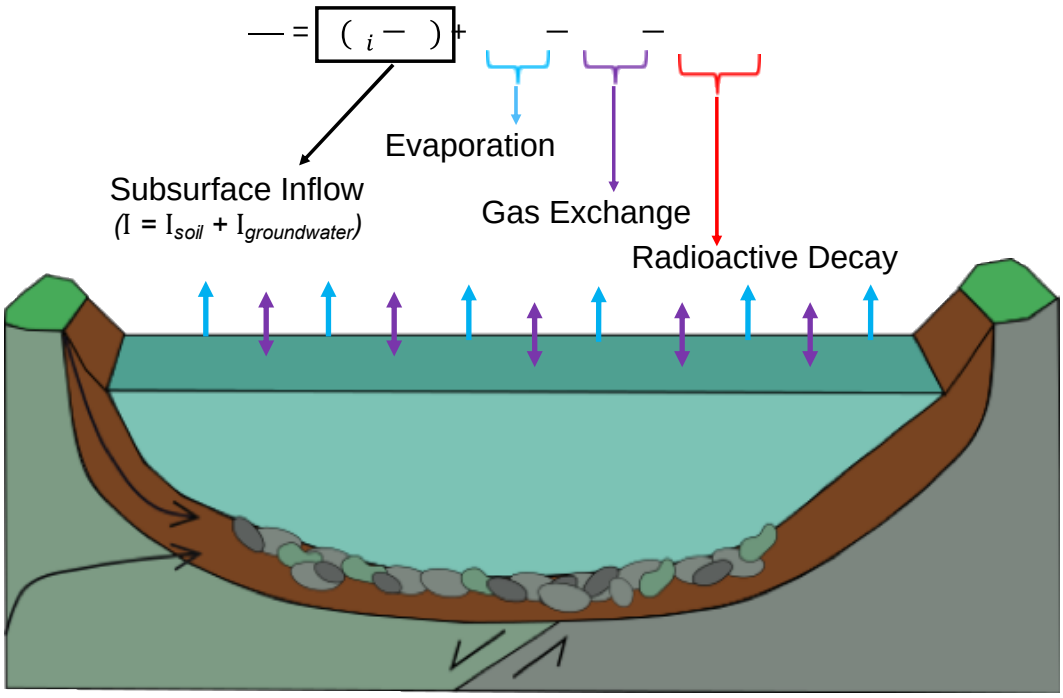


*Figure 4. A schematic stream cross section showing all of the processes accounted for in the equation used in $^{222}$Rn modeling.*

To evaluate incremental gains in subsurface sources at each stilling well, fractions of subsurface discharge to total streamflow ($F_{ss}$) were calculated in the following manner:

$$F_{ss} = \frac{Q_{ss_1} - Q_{ss_2}}{\Delta Q_t} \quad (6)$$

where $Q_{ss_1}$ is the upstream modeled subsurface discharge (L/s), $Q_{ss_2}$ is the downstream modeled subsurface discharge (L/s), and $\Delta Q_t$ is the difference in measured total streamflow from upstream to downstream (L/s).

The parameters used for radon modeling are shown in **Table 2**. Parameters that were not directly measured in the field were estimated based on a series of equations detailed in **Table 2**. Following the approach of Cook *et al*. (2003) sensitivity analysis was conducted by varying a model parameter by ± 50% while keeping the other parameters constant to see the effect that the varied parameter had on subsurface inflow. Particular interest was given to the parameters that were not measured in the field since they were the largest source of uncertainty in the model.

Gas transfer velocity (*k*) is difficult to constrain in low-order mountainous streams with variable geometries, velocities, and temperatures. Accordingly, special attention was given to the effect of varied *k* on estimated subsurface inflow rates. Four common equations that depend on slope, velocity, and depth (O'Connor and Dobbins, 1958; Negulescu and Rojanski, 1969; Raymond *et al.*, 2012) were used to approximate the gas transfer velocity in a nearby catchment (Brisette, 2017). These values were adopted in our study and used as a proxy for *k* in CWW because of topographical similarities and geographical proximity between the two catchments.

*Table 2. Details parameters used in $^{222}Rn$ modeling.*

| ***Parameter*** | ***Units*** | ***Value(s)*** | ***Method of Collection or Estimation*** |
|---|---|---|---|
| In-Stream Radon Concentration (*c*) | (Bq/L) | Avg. 0.907;<br>0.074 – 4.64 ±15% | Measured in field and analyzed using the RAD7 Alpha Decay Spectrometer at the University of Montana; longitudinally and temporally variable |
| Total River Length (*x)* | (km) | 5 | Measured in field |
| Evaporation Rate (*E)* | (mm/day) | 0 | Assumed negligible (Cook *et al.*, 2006) |
| Initial Radon Concentration (*c*) | (Bq/L) | Avg. 0.37;<br>0.12 – 0.60 ±15% | Concentration of most upstream sampling location (variable); measured in field |
| Atmospheric Radon Concentration | (Bq/L) | 0 | Assumed negligible (Cook *et al.*, 2006) |
| Radon Decay Coefficient (λ) | (/day) | 0.18 | Constant |
| Gas Transfer Velocity (*k)* | (m/day) | Avg. 16.6<br>5.5 – 27.7 | Estimated from a suite of equations detailed in Brisette, 2017 |
| Groundwater Inflow Concentrations ($c_i$) | (Bq/L) | 32.0 | Highest measured concentration of groundwater samples; measured in field and analyzed using the RAD7 Alpha Decay Spectrometer at the University of Montana |
| Stream Width (*w*) | (m) | 0.75 | Measured in field |
| Stream Depth (*d*) | (m) | 0.15 | Measured in field |

### *3.3.2 End-Member Mixing Analysis (EMMA)*

EMMA is a method of reducing the dimensionality of a multivariate geochemical dataset by eigenvector-decomposition to identify the correct number and source of end-members that significantly contribute to streamflow generation. The dataset is reduced into 'principal components,' which represent orthogonal, linear combinations of chemical species that span data variance. Stream and potential end-member sample data are projected on a subset of components that span the majority of variance to reduce the data dimensionality and then reanalyzed by a series of diagnostic tests detailed below. With data in terms of mixing subspace coordinates,

stream and end-member sample compositions were reprojected to concentrations of the original solutes and used to assess end-member contribution to streamflow.

Unlike traditional hydrograph separations, where initial assumptions are required regarding the number and chemistry of end-members, EMMA assesses the minimum number of geochemical combinations (or dimensions) needed to explain the variability in the data. The number of dimensions is directly related to the number of end-members that explain the variance in runoff chemistry (Hooper, 2003). Thus, this method identifies the appropriate number of end-members directly, reducing subjective choices. Additionally, while mass-balance approaches require the prior knowledge of end-member geographical source, EMMA screens each end-member candidate for appropriateness of fit, helping to reduce user bias when creating mixing models. Lastly, EMMA determines whether or not initial model assumptions are violated by identifying whether or not a 'good mixing subspace' is achieved. If a 'good mixing subspace' is unobtainable within the chemical dataset, it may indicate non-conservative tracer behavior.

End-member mixing analysis was performed following the approach of Hooper (2003). Stream chemistry was normalized by subtracting the sample mean and dividing by the standard deviation of each solute. The normalized data were arranged in an $n$ x $p$ matrix, for the $n$ stream samples and $p$ chemical species. Next, a principal component analysis was performed on the sample matrix, which is analogous to spectral decomposition of the data covariance, which determines an orthogonal set of eigenvectors and associated eigenvalues which span the covariance matrix. The eigenvalue associated with a given eigenvector represents the amount of variability explained by or the "loading" of the associated eigenvector which represents a linear combination of chemical species. The magnitude of eigenvalues was used to determine the dimensionality of the mixing sub-space. The number of retained vectors were chosen such that

the majority of variance in the data is explained by as few eigenvectors as possible. To evaluate the percent of variability explained by each eigenvector, individual eigenvalues were divided by the sum of all eigenvalues (**table 2-A** in the appendix). In this study, the first three eigenvalues explained ~90% of variance in the data. The remaining variance in the dataset unexplained by the first three eigenvalues is assumed to be related to 1) noise within the dataset and 2) end-members that do not significantly contribute to streamflow.

Chemical samples from potential end-member waters (e.g. soil and groundwater) were standardized by the mean and standard deviation derived from stream chemistry and projected into the lower dimensional mixing sub-space determined from the stream samples alone. Following Christophersen *et al.* (1992), the composition of EMMA end members was chosen based upon this principal component projection. In a 2D plot, the end-members should bound the stream samples in a 'convex' sense.

Residual values, calculated as the difference between observed solute and reprojected concentrations, were then calculated to 1) check end-member picks in a more quantitative sense against their visual geometric projection and 2) ascertain whether or not the stream chemistry was projected into a 'good mixing subspace.' Well posed end-members exhibit small residual values. For all stream samples, residuals were plotted against original chemical data. A 'good mixing subspace' is indicated by a lack of structure in the plot, which indicates that no major assumptions were violated (i.e. non-conservative tracer behavior) (Hooper *et al*., 2003).

Each stream sample and end-member composition was then reprojected back into the original solute space using the only the selected number of eigenvectors. With all data expressed in terms of original solutes, mass-balance mixing models were used to understand end-member

contribution to streamflow on spatial and temporal scales. The general mass balance equations for a *j*th-component mixing model are given by:

$$\begin{bmatrix} 1 & 1 & 1 \\ C_1^1 & \dots & C_j^1 \\ \vdots & \ddots & \vdots \\ C_1^i & \dots & C_j^i \end{bmatrix} \cdot \begin{bmatrix} Q_1 \\ \vdots \\ Q_j \end{bmatrix} = \begin{bmatrix} Q_t \\ Q_t C_1^1 \\ \vdots \\ Q_t C_j^i \end{bmatrix}$$

$$A \cdot \vec{Q} = \vec{D}$$

where $C_j^i$ is the concentration of the *i*th tracer in the *j*th end-member, and $Q_j$ is the discharge of the *j*th end-member. To solve for the discharge of each component:

$$\vec{Q} = A^{-1}\vec{D}$$

Subject to $Q_j >= 0$

where $A^{-1}$ is the inverse of matrix $A$. A minimum of *n* tracers are required to solve for *n+1* end-members, given the discharge mass balance equation. Here, we used four tracers to constrain a two-component mixing model where soil water and groundwater were end-members. Justification for these end-members is discussed in greater detail in the results section (*4.2 End-Member Mixing Analysis*). Chemical concentrations used in these mixing models are detailed in **table 1-A** in the appendix. Mixing model interpretations were then checked by multiplying the results of mass-balance separations (in terms of a fraction) by the original solute concentrations of end-members to see how accurately stream chemistry was reproduced.

### *3.3.3 Terrain Analysis*

In order to explore topographic characteristics that influence stream flow generation and source, the catchment was delineated into 'sub-catchments' to de-aggregate hillslope contributions. Beginning with a 10m resolution digital elevation model of LEF, watershed boundaries of CWW were delineated by creating flow direction and accumulation grids to determine how water is routed within the catchment based on topography. The watershed was

then divided into seven sub-catchments based on the contributing area to each stilling well (**figure 5**). Polygons outlining each sub-catchment were imported into SAGA GIS where the mean elevation, TWI, and catchment area were calculated for each sub-catchment. Linear regression was then performed to assess modeled end-member discharge correlation to terrain attributes in an 'incremental' and 'cumulative' sense.

To analyze the relationship between landscape and end-member discharge in an 'incremental' sense, fractions of end-member discharge gained in each sub-catchment were calculated by quantifying the solute concentration of water entering the incremental reach ($\Delta C$) at each stilling well along the reach using:

$$\Delta C = \frac{Q_d C_d - Q_u C_u}{\Delta Q} \quad (7)$$

where $Q_d$ is downstream discharge (L/s), $C_d$ is downstream solute concentration (mg/L), $Q_u$ is upstream discharge (L/s), $C_u$ is upstream solute concentration (mg/L), and $\Delta Q$ is the net change in discharge from the upstream stilling well to the downstream stilling well (L/s). Incremental solute concentrations were calculated for each tracer used in mixing models (calcium, magnesium, sodium, and chloride). These solute concentrations were used in mass-balance mixing models to quantify fractional gains in groundwater and soil water from one sub-catchment to the next. Modeled end-member fractions were compared against the mean elevation and TWI values as well as area for each sub-catchment to evaluate the relationship among internal catchment characteristics and discharge.

To evaluate these relationships in a 'cumulative' sense, the mean elevation and TWI from each sub-catchment were made into cumulative averages with increasing distance downstream that incorporated data from successive sub-catchments. The cumulative elevation, TWI, and UAA values were then compared against original EMMA-modeled groundwater and

soil water fractions at each stilling well location. These analyses were conducted for each synoptic sampling campaign to evaluate seasonal change.

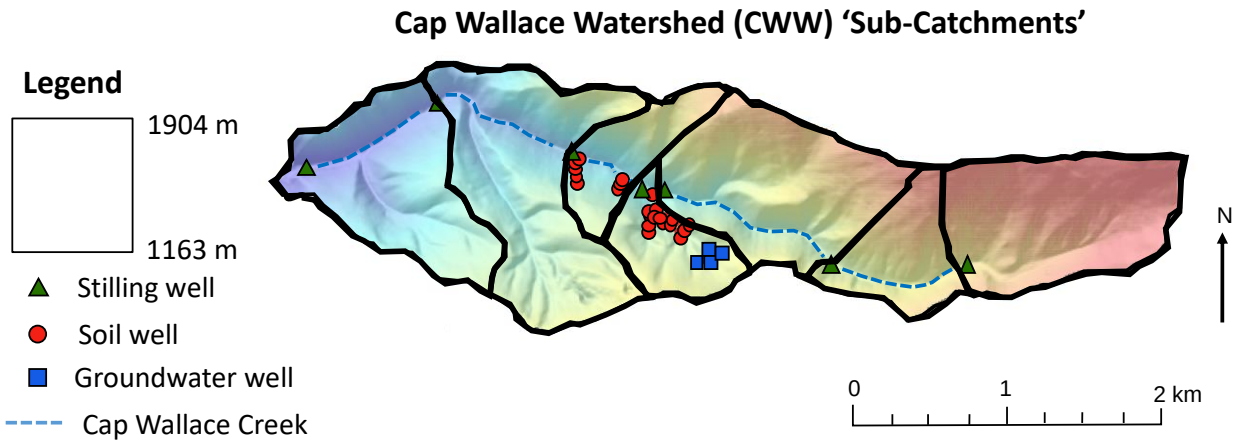


*Figure 5. 'Sub-catchments' (outlined in black) delineated by contributing areas of stilling wells in CWW. The sub-catchments are superimposed on top of a 10m resolution DEM of CWW.*

## 4. Results

### *4.1 Radon Modeling*

Samples collected for radon activity were taken at each of the seven stilling well locations throughout variable flow states. Duplicate samples were within 0-40% of one another with larger variability observed in low concentration samples consistent with Poisson statistics of radio-active decay. Duplicate samples with higher concentrations were within 2-3% of one another showing good repeatability. At a concentration of 0.074 Bq/L (corresponding duplicate of 0.111 Bq/L), for example, a 40% variability was observed. At a concentration of 2.527 Bq/L (duplicate 2.597 Bq/L) a 2.7% variability was observed. Radon concentrations and observed discharge are shown in **figure 6**. Radon concentrations ranged from 0.074 to 4.25 Bq/L, but showed the same spatial pattern across varying discharges (**figure 6**). During each sampling

period, a large increase in radon activity was observed approximately half way down the observed reach (~2.5 km).

Despite seasonal variability in observed stream discharge and $^{222}Rn$ concentrations, estimated subsurface inflows are shown to be primarily responsible for the gain in streamflow along the entire observed reach throughout the year. **Figure 7** shows estimated subsurface discharge against both modeled and observed total stream discharge. The longitudinal profile of subsurface discharge closely follows total stream discharge, indicating that the gain in streamflow is predominantly from subsurface sources. Subsurface discharge accounted for 19-100% of the incremental gains in streamflow but averaged 81% (**figure 8**). May and mid-June were estimated to have stronger influences of non-subsurface discharge with subsurface discharge accounting for 68% and 59% of the incremental gains in streamflow, respectively. Along the reach, non-subsurface discharge generation was estimated to have occurred near the center of the reach (2.5-3 km downstream of the headwaters) at the convergence of two large hillslopes.

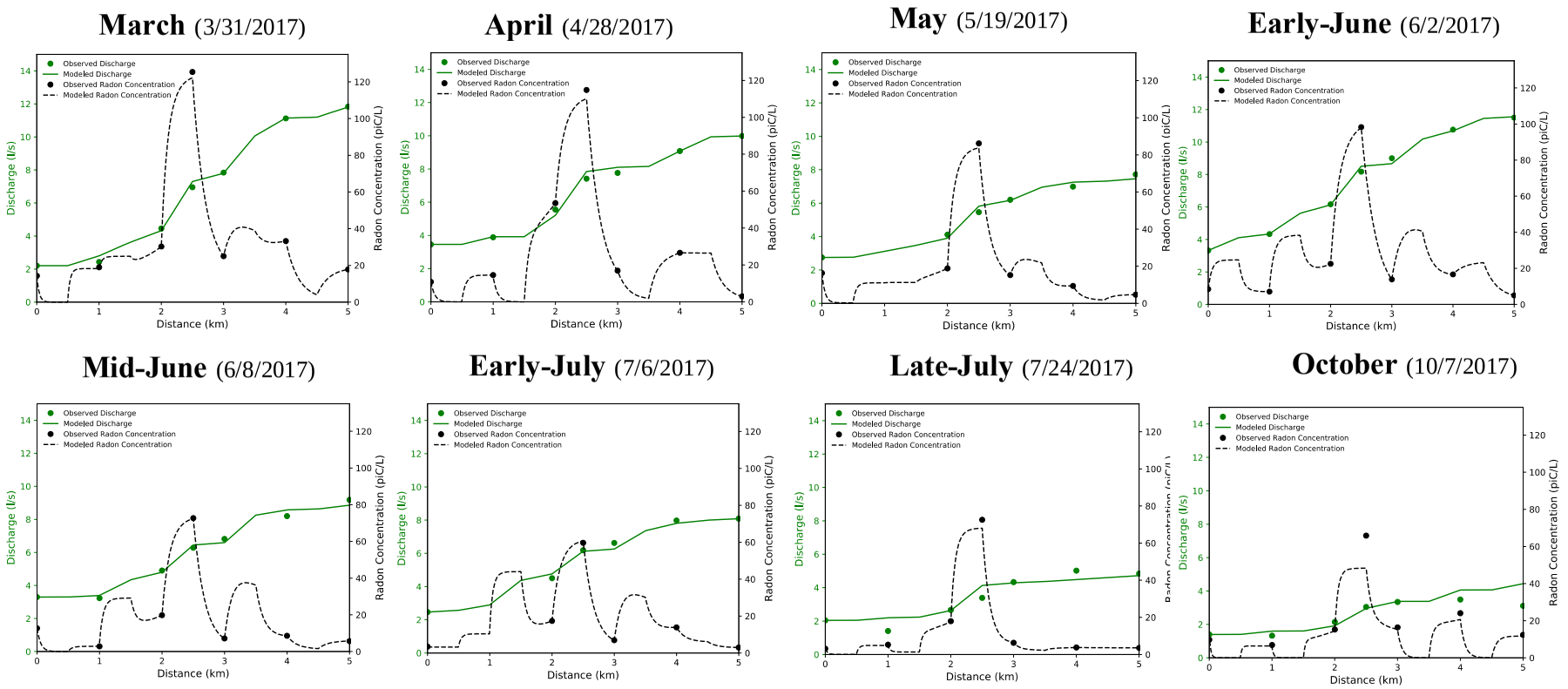


*Figure 6. Longitudinal profiles of measured and modeled $^{222}$Rn concentrations and stream discharge. Black and green dots represent measured in stream $^{222}$Rn concentrations and discharge, respectively. Dashed black and green lines represent modeled $^{222}$Rn concentration and stream discharge, respectively. Modeled results are closely aligned with measured data.*

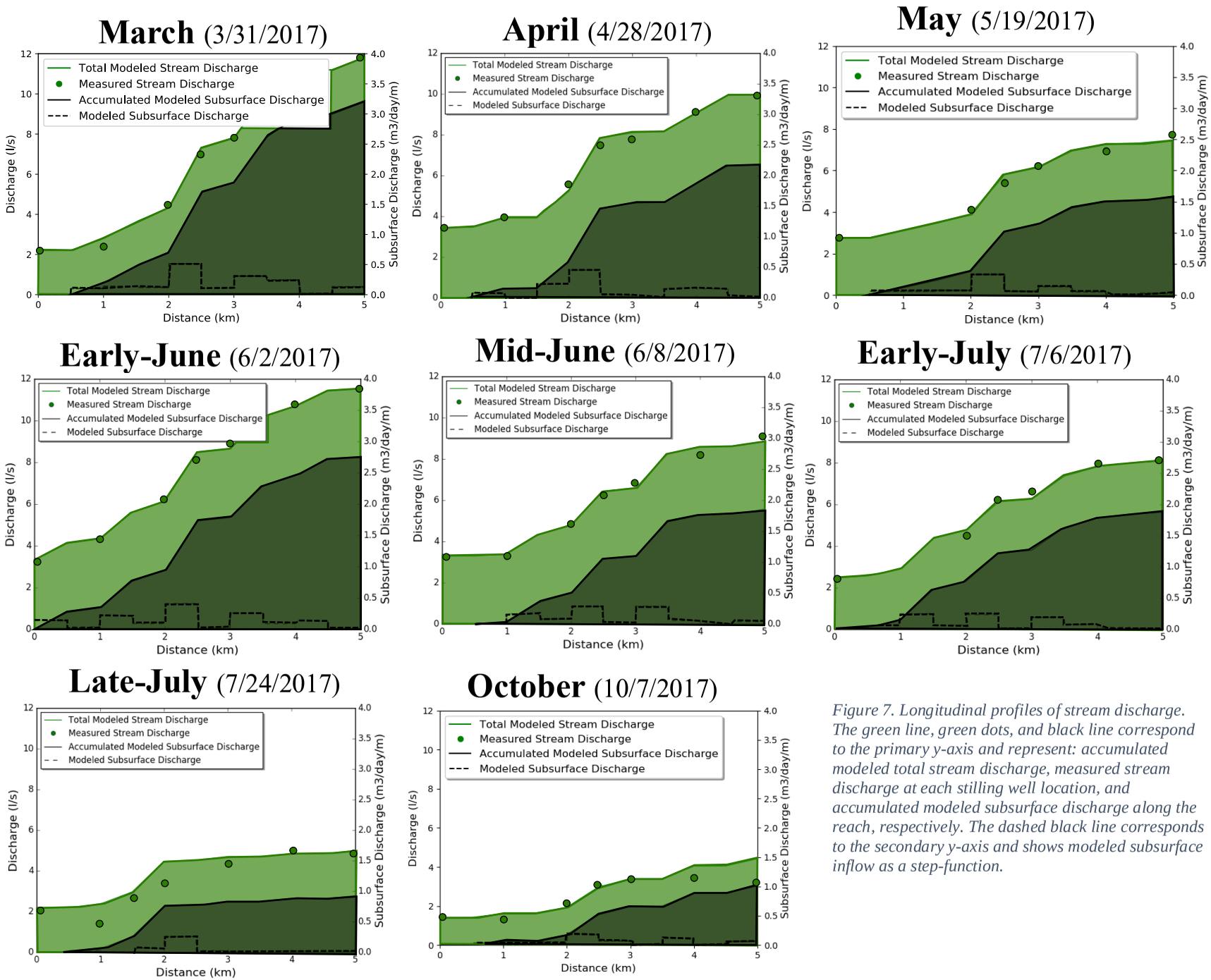


*Figure 7. Longitudinal profiles of stream discharge. The green line, green dots, and black line correspond to the primary y-axis and represent: accumulated modeled total stream discharge, measured stream discharge at each stilling well location, and accumulated modeled subsurface discharge along the reach, respectively. The dashed black line corresponds to the secondary y-axis and shows modeled subsurface inflow as a step-function.*

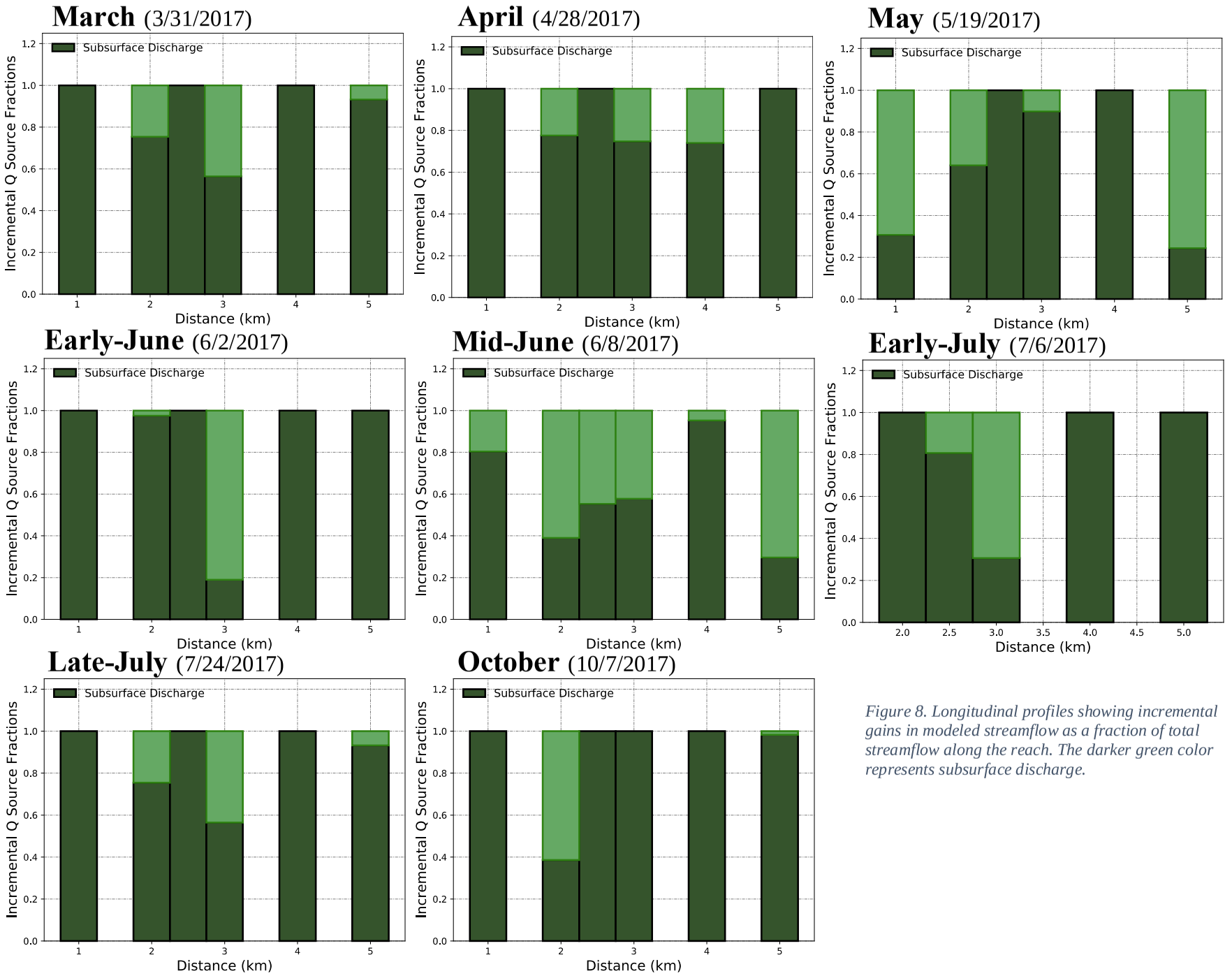


*Figure 8. Longitudinal profiles showing incremental gains in modeled streamflow as a fraction of total streamflow along the reach. The darker green color represents subsurface discharge.*

### *4.2 End-Member Mixing Analysis*

Three principal components spanned ~90% of the data variability, and a 3D mixing subspace was deemed to appropriately fit the stream and end-member chemistry. Following Hooper (2003), the dimensionality of the mixing subspace was determined by 1) the percentage of variance explained by the first three eigenvalues (**table 2-A** in the appendix) and 2) the lack of structure in the plots of residual EMMA projections against original stream chemistry, indicating that a 'good mixing subspace' was achieved (**figure 9**). The following 3 equations explain the contribution of each solute identified in the principal component analysis for each component in the mixing subspace:

$PC_1 =$ 0.42 Ca + 0.04 K - 0.18 Mg + 0.09 Na + 0.28 F + 0.83 Cl - 0.10 SO4 - 0.10 NO3

$PC_2 =$ 0.31 Ca + 0.45 K - 0.01 Mg - 0.25 Na + 0.13 F - 0.12 Cl + 0.16 SO4 + 0.43 NO3

$PC_3 =$ 0.40 Ca - 0.06 K - 0.23 Mg + 0.25 Na + 0.31 F - 0.32 Cl + 0.65 SO4 - 0.13 NO3.

End-members were chosen based on the 2D EMMA mixing subspace plot (**figure 10**). Average groundwater and soil water (within the headwater stream samples) were chosen as end-members because the majority of stream chemistry plotted in between the two indicating that their chemistry could be reproduced by some combination of the two end-members.

All samples and end members were reprojected into chemical species and mixing analysis performed. The fraction of soil and groundwater end-members in stream water samples are summarized in **figure 11**. In general, groundwater becomes a larger component of streamflow with increasing distance downstream. **Figure 12** shows how the percentage of groundwater at the outlet changes as a function of time. The fraction of groundwater to total streamflow at the outlet was highest during the late spring (June 2$^{nd}$, 2017) and lowest during mid-spring (May 19$^{th}$, 2017). Groundwater at the outlet fluctuated between 26-44% and averaged 38% of total stream flow.

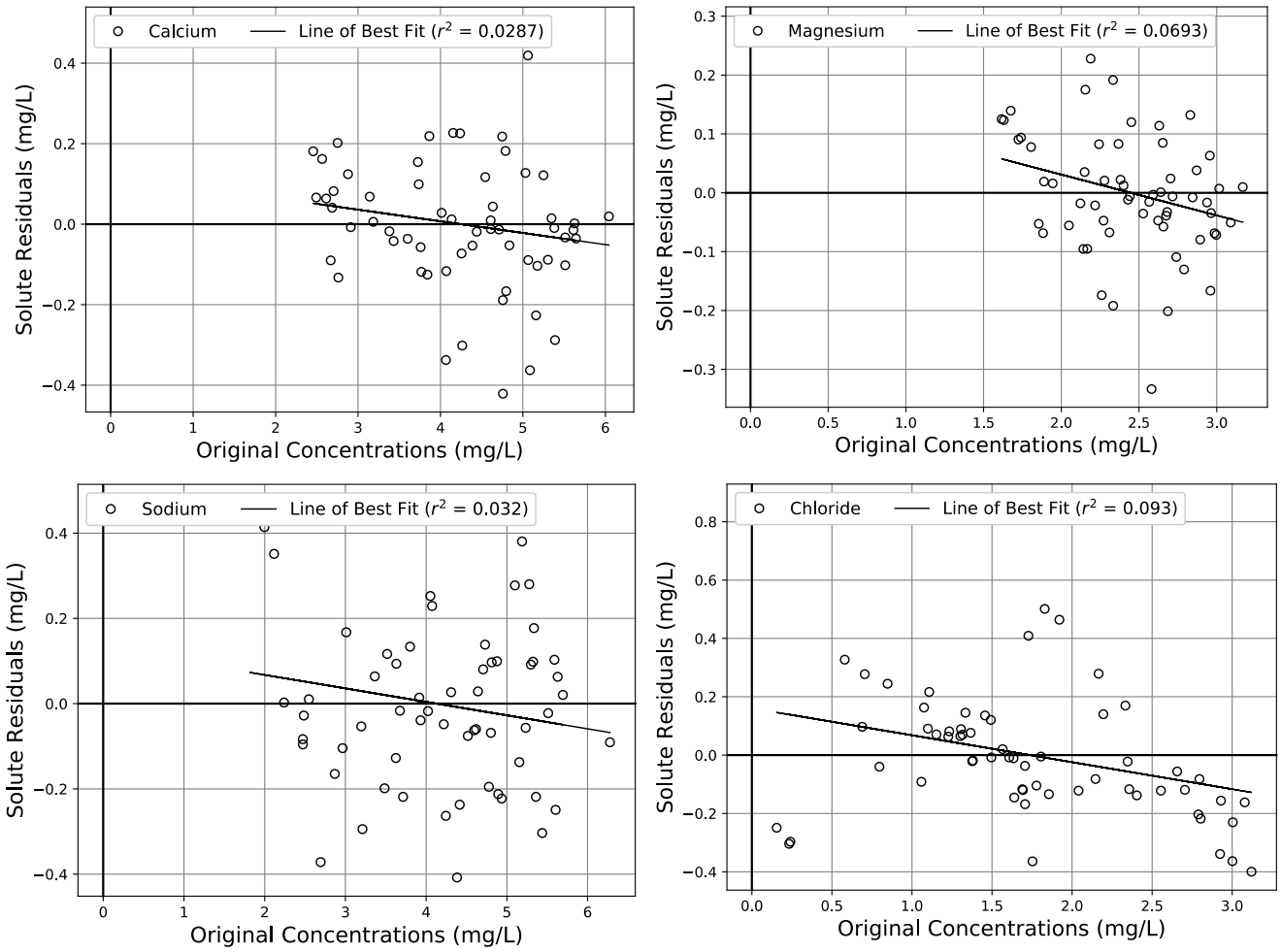


*Figure 9. Plots of residual solute concentrations from EMMA projections against original solute concentrations for the tracers used in mass-balance mixing models.*

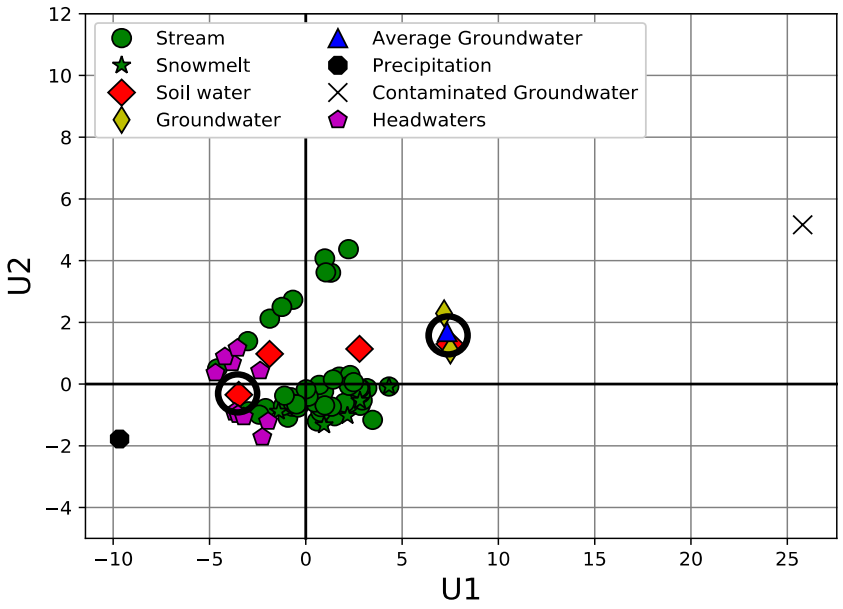


*Figure 10. A 2D EMMA mixing subspace projection of stream and end-member chemistry. Soil water and average groundwater (circled in black) show our choice in end-members.*

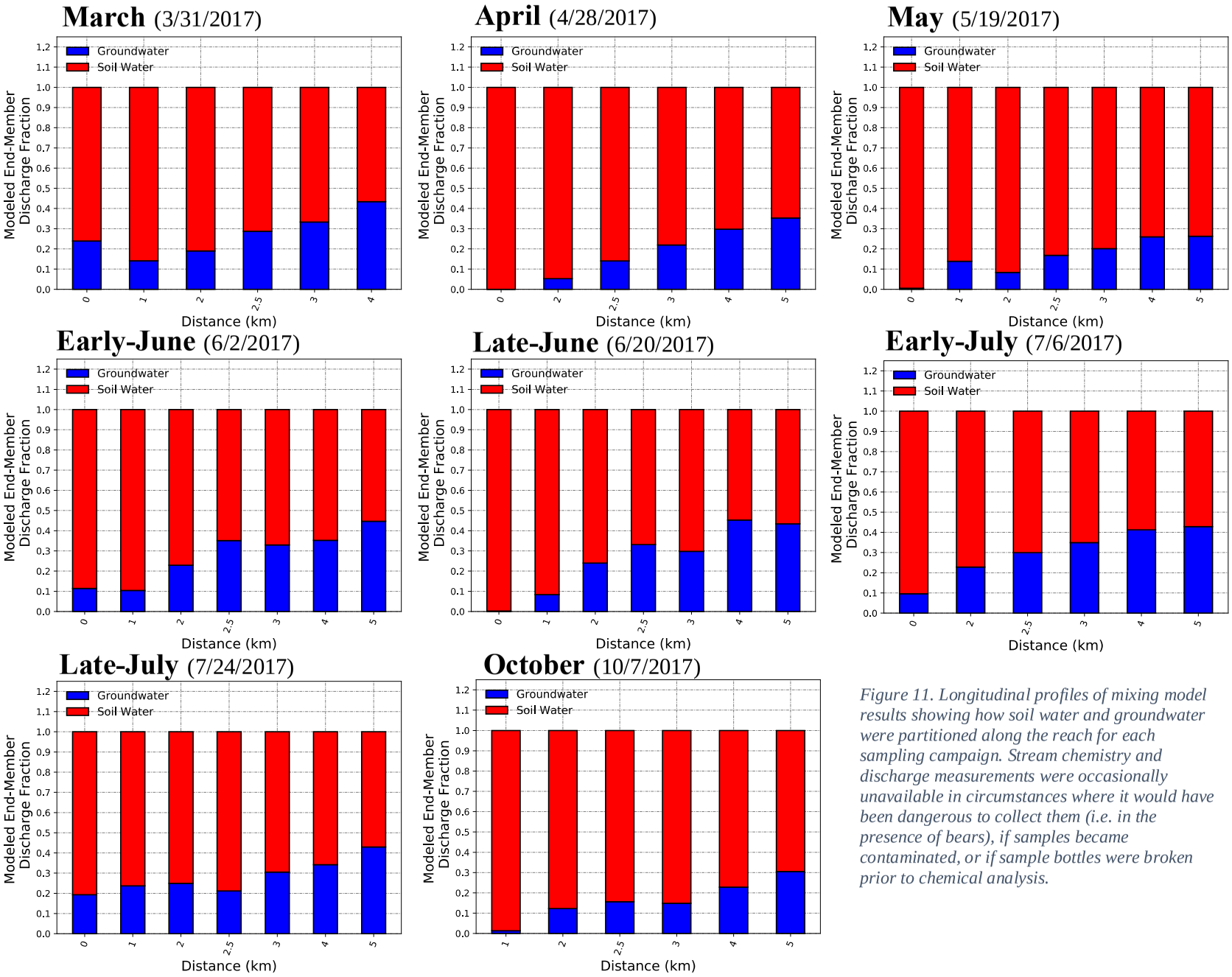


*Figure 11. Longitudinal profiles of mixing model results showing how soil water and groundwater were partitioned along the reach for each sampling campaign. Stream chemistry and discharge measurements were occasionally unavailable in circumstances where it would have been dangerous to collect them (i.e. in the presence of bears), if samples became contaminated, or if sample bottles were broken prior to chemical analysis.*

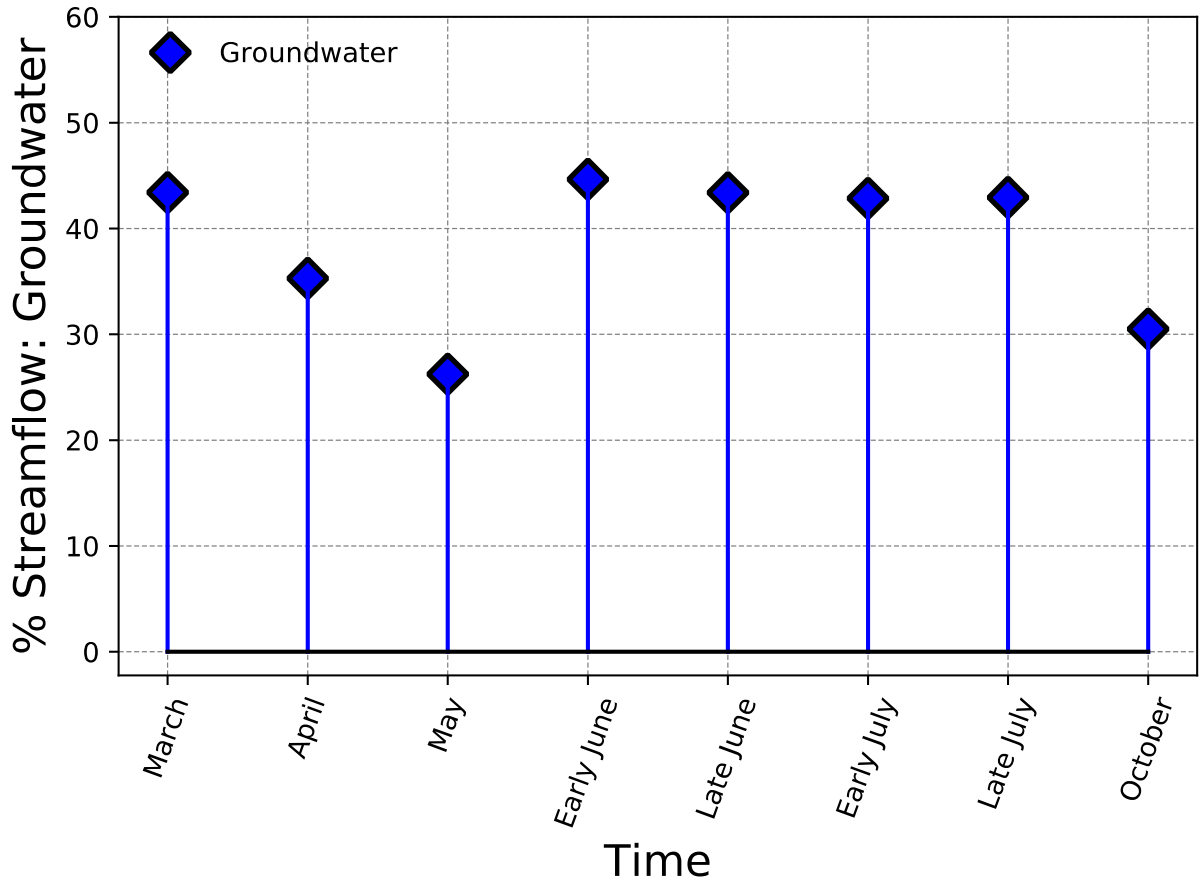


*Figure 12. Seasonal fluctuation of groundwater fraction of total streamflow at the outlet.*

### *4.3 Terrain Analysis*

Linear regression of cumulative mean terrain indices and soil and groundwater fractions revealed strong relationships between cumulative average elevation and upslope accumulated area against end-member contributions (**figure 13**). $R^2$ values ranged from 0.52 to 0.98 over the seven-month period in 2017. No systematic trend was found among incremental end-member discharges and incremental mean terrain indices (**figure 14**). $R^2$ values ranged from 0.05 to 0.81 but tended to switch drastically from high to low values.

Hydrometric data from soil wells located at various landscape positions were used as a proxy for determining when the catchment was 'wet' by showing the interconnectedness of the water table over time. Soil water connection was evaluated through binary plots of saturated vs.

unsaturated conditions. Soil wells with high TWI values tended to stay continually saturated where soil wells with lower TWI values exhibited more transient-like behavior in response to climatic forcing. $R^2$ values from cumulative and incremental regression are plotted with binary soil well responses in **figure 15** as a function of time. In both cases, the $r^2$ value was highest (0.98 and 0.81, respectively) in early July, approximately 3 weeks after the largest catchment 'wet-up.'

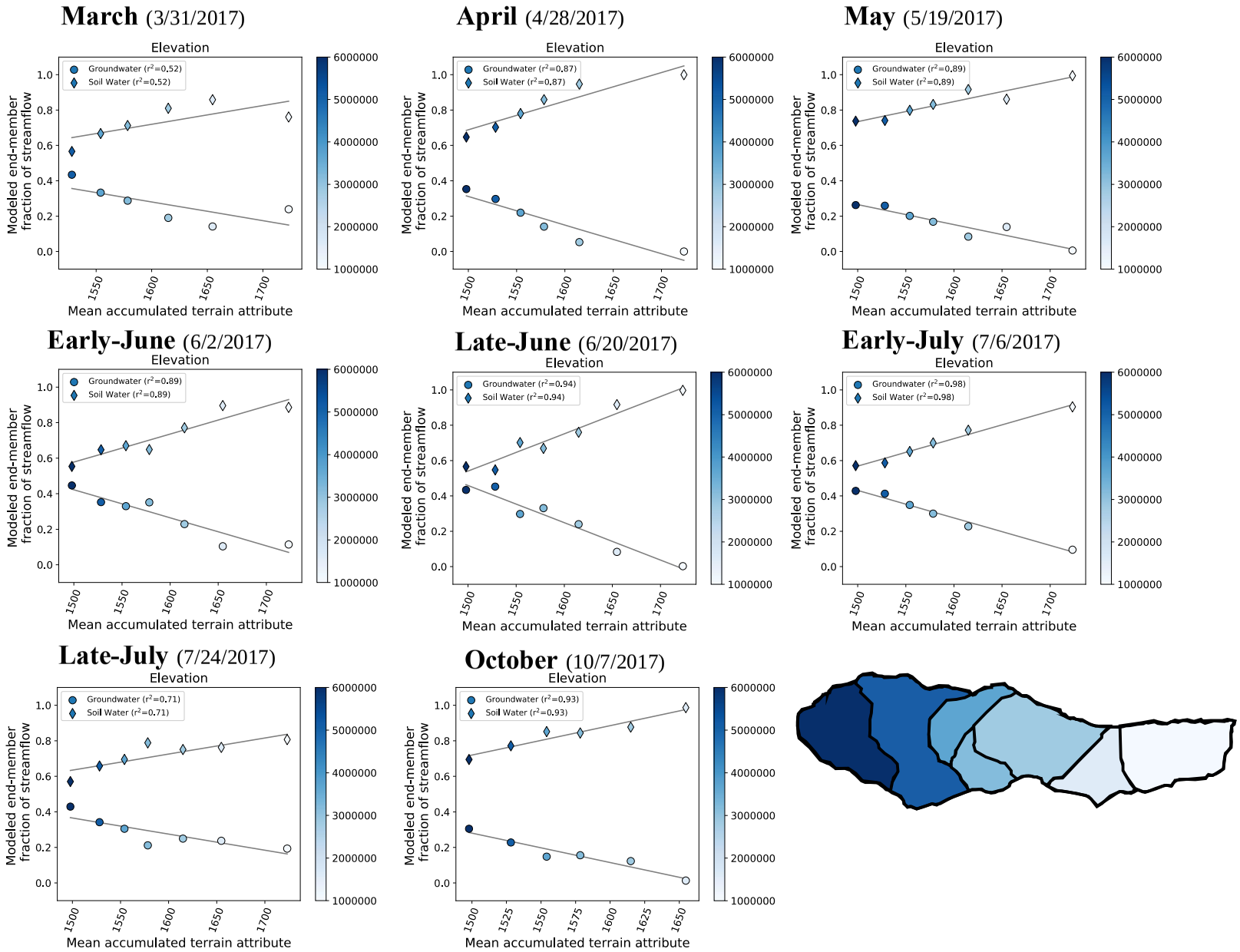


*Figure 13. Regression results from cumulative analysis of end-member discharge against elevation and UAA. Blue dots and diamonds are color coordinated with cumulative mean UAA to show relative fractions of modeled groundwater and soil water discharge along the reach, respectively. The CWW inset on the bottom right shows catchment area aligned with the color scheme of blue dots and diamonds.*

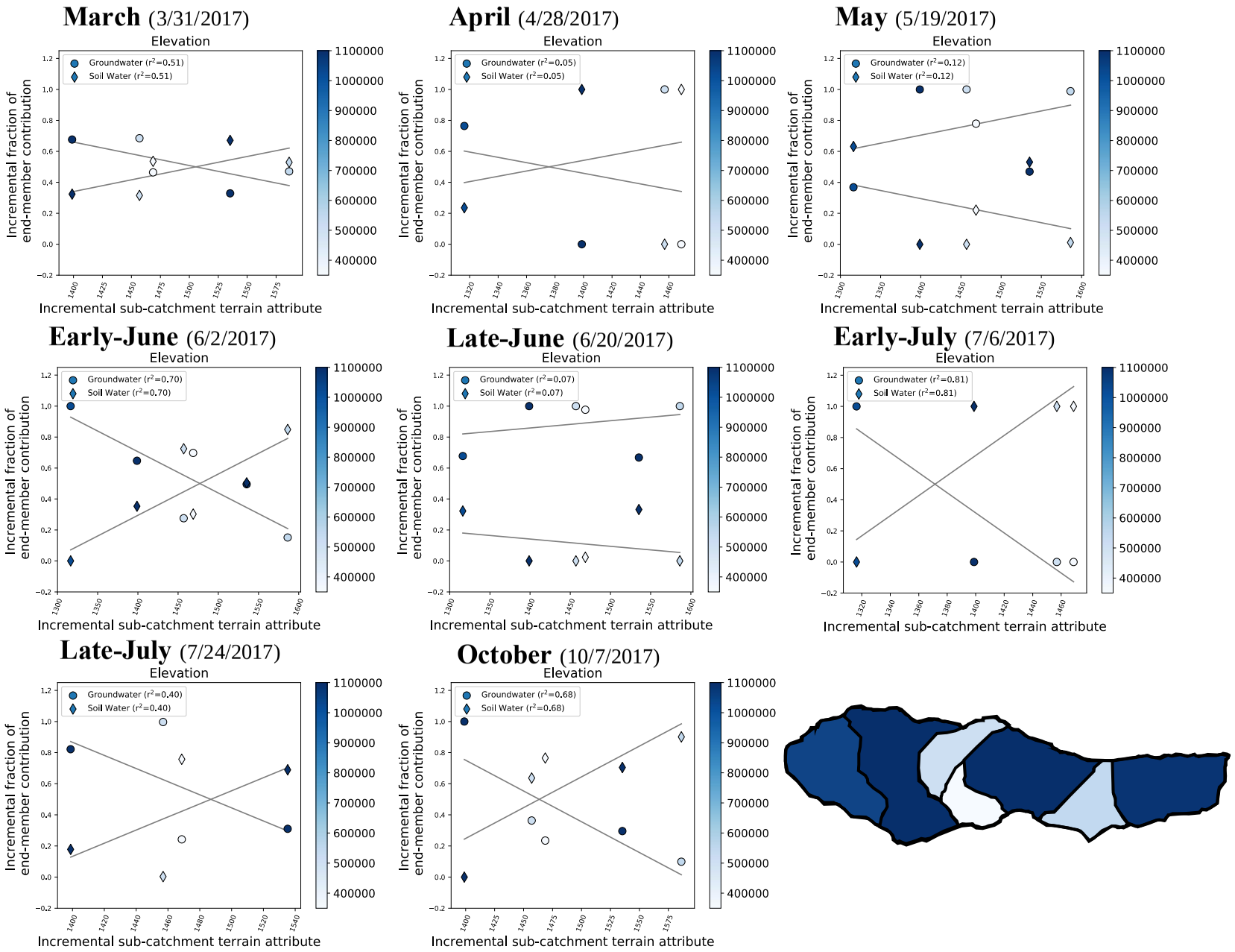


*Figure 14. Regression results from incremental analysis of end-member discharge against elevation and UAA. Blue dots and diamonds are color coordinated with sub-catchment area to show relative incremental fractions of modeled groundwater and soil water discharge, respectively. The CWW inset on the bottom right shows sub-catchment area aligned with the color scheme of blue dots and diamonds.*

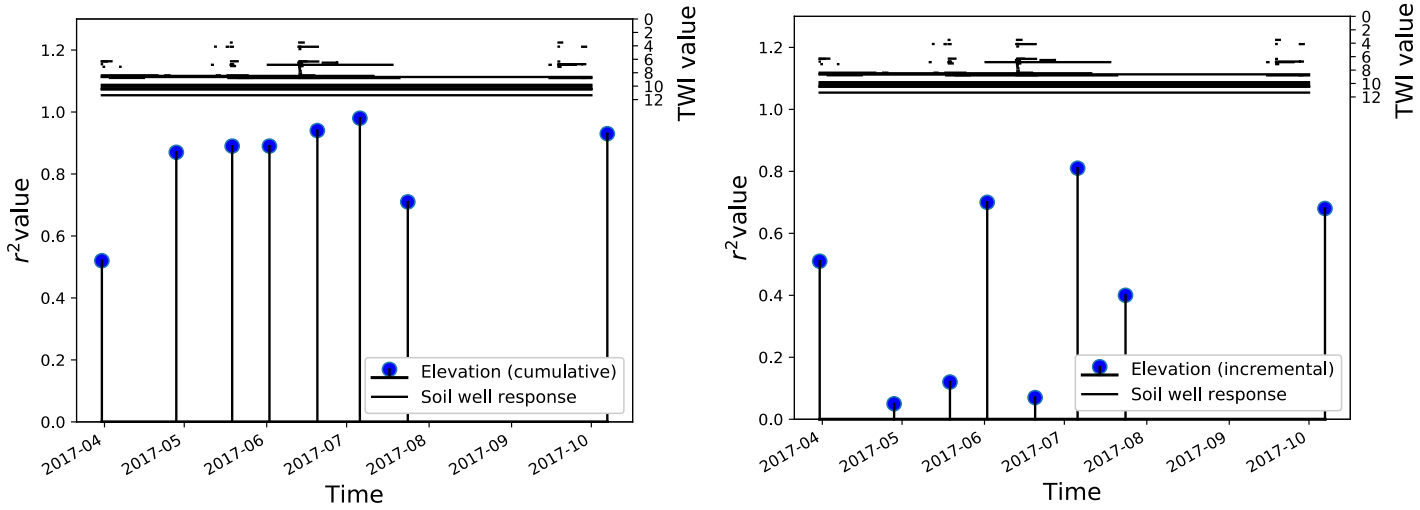


*Figure 15. Blue dots show the $r^2$ values from cumulative and incremental regression of elevation values against modeled end-member fractions through time. The black lines near the top of the plot are binary soil well responses with corresponding TWI values in which the length of the line corresponds to the amount of time a soil well was saturated. The table above summarizes the $r^2$ values from cumulative and incremental regression.*

*Table 3. A summary of $r^2$values from cumulative and incremental regression (figures 14).*

| | ***March*** | ***April*** | ***May*** | ***Early June*** | ***Late June*** | ***Early July*** | ***Late July*** | ***October*** |
|---|---|---|---|---|---|---|---|---|
| Elevation (*cumulative*) | 0.52 | 0.87 | 0.89 | 0.89 | 0.94 | 0.98 | 0.71 | 0.93 |
| Elevation (*incremental*) | 0.51 | 0.05 | 0.12 | 0.70 | 0.07 | 0.81 | 0.40 | 0.68 |

## Discussion

### *5.1 Radon Modeling*

Radon modeling suggests that along the reach, gains in streamflow are driven by subsurface discharge for all times sampled, which implies that the majority of runoff is derived from subsurface sources in Cap Wallace Creek throughout the year. While previous research has found subsurface discharge to be an important source of streamflow after storms or during baseflow (e.g. Sklash *et al*., 1975; Hooper & Shoemaker, 1986; McDonnell *et al*., 1991), our study showed that subsurface discharge is the main driver of streamflow, throughout the snowmelt cycle across variable discharges. This work is particularly beneficial for understanding how snowpack is routed to the stream network and potential for storage in subsurface reservoirs, which has implications for understanding watershed response to climate change.

While incremental discharge source plots show that subsurface sources account for the majority of streamflow gain, there are some instances in which non-subsurface sources are estimated to be more important in streamflow generation (**figure 8**). Non-subsurface streamflow generation occurred throughout the year but had the strongest influence on stream chemistry during the late spring to mid-summer (May through late July). These instances occurred mostly in the middle of the reach where there are multiple convergent zones from large hillslopes (**figure 5**). For example, on June 8$^{th}$, 2017 a 0.25 L/s increase in streamflow was recorded from stilling well 'CWSTW6' (located approximately 2.5 km downstream from headwaters) to stilling well 'CWSTW2-upper' (~3 km downstream from headwaters). Over this same reach, a 0.15 L/s increase in modeled subsurface discharge was calculated, implying that 60% of discharge gained came from the subsurface while 40% came from the surface. It is important, however, to view these results in light of 1) the magnitude of discharge increments, 2) uncertainty in the parameters used to quantify groundwater inflows and 3) the transit time of subsurface discharge and resulting radon concentration.

In the example above, the magnitude of flow increase was small compared to the uncertainty in discharge and modeled subsurface inflow. Groundwater inflow estimates derived from $^{222}$Rn are sensitive to the gas transfer velocity ($k$) which is also one of the least constrained parameters in the radon transport model. Varying the gas transfer velocity by ± 50% has a marked effect on estimated groundwater inflow. A 50% decrease in the gas transfer velocity would result in a model estimated gain 0.0 L/s implying that 100% of streamflow comes from the surface. In contrast, a 50% increase in gas transfer velocity would results in a model estimated gain of 0.45 L/s more than what was actually measured.

Additionally, radon modeling is limited to detecting subsurface sources that has appreciably high concentration of $^{222}$Rn, which requires subsurface residence times over a couple days. Secular equilibrium is reached after approximately two weeks. It is possible that subsurface sources with brief residence times and thus low $^{222}$Rn concentration could go undetected. Hydrometric data from soil wells shows that the catchment was most wet in May – July (**figure 15**). This is the same period that surface water had the strongest influence on streamflow generation. **Figure 15** shows that soil wells with low TWI values (generally located at higher elevations with less accumulated area) exhibit transient behavior to catchment wet-ups. Some wet-ups were on the order of hours to days, suggesting that soil water at these landscape positions is lost quickly through lateral flow or infiltration to the bedrock aquifer. Quick residence times associated with transient behavior could provide explanation for why subsurface sources may have entered the stream undetected during the wet months.

### *5.2 End-Member Mixing Analysis*

End-member mixing analysis provided an independent test of discharge source, and the ability to further divide stream-flow composition. EMMA indicated that most streamflow interacts with the subsurface before reaching the stream, consistent with $^{222}$Rn results. EMMA, however, was able to shed light on how streamflow was partitioned between soil water and groundwater components. EMMA indicates that the stream is generally composed of soil water at the headwaters, but groundwater discharge increases with downstream distance even during snowmelt and heavy rainfall. This observation contradicts a 'Teflon-surface' watershed conceptual model, in which precipitation and snowmelt are routed downslope to the stream network through the soil layer, while the bedrock acts as an impermeable surface. Increasing influence of groundwater with downstream distance argues for a 3D watershed conceptual model consistent with the findings of Frisbee *et al*. (2011) and Frisbee *et al*. (2012). However, while

other studies have suggested that regional groundwater flowpaths are of increasing importance with increasing catchment scale (Frisbee *et al*., 2011; Frisbee *et al*., 2012), this study show this relationship exists even on small-scale headwater catchments.

The temporal analysis indicates little variability in modeled end-member proportions throughout the observed time period; however, early summer months have the highest groundwater discharge proportions. Several large precipitation events (~60 mm/day) occurred in early June. It appears these precipitation events rapidly loaded the subsurface reservoirs which could be driven by a variety of mechanisms including the 'capillary-fringe' effect. Here results indicate that the groundwater system rapidly reacts to precipitation inputs consistent with experimental observations of Anderson *et al.* (1997). While the capillary fringe mechanism explains the larger fraction of groundwater discharge during the early summer months, our observed late-season groundwater ratios of streamflow counter what has typically been observed by other researchers. Several previous hydrograph separation studies have assumed baseflow to be entirely composed of groundwater (e.g. Pinder & Jones, 1969; Genereux *et al.*, 1993), while our results indicate that soil water is a substantial portion of streamflow during that time. Again these results align better with the results of Anderson (1997), which indicate a more rapid response and a more long-term storage release from soil flow.

A principal source of error in the EMMA derived results is the assumption of constant end-member concentration. In the 2D EMMA mixing subspace plot (**figure 10**), late season stream chemistry follows a different trajectory than spring and early summer stream chemistry which could be indicative of a change in end-member chemistry. Because groundwater composition is a function of flow velocity, residence time, rate of kinetic mineral weathering, and available surface area of weatherable material, it is likely that the groundwater discharging

to the stream later in the late season has longer residence times and as a consequence a more evolved chemical signature. Mixing calculations were completed with an average groundwater composition from samples collected in the late spring when the water table was high. Thus, the late summer mixing model results may not accurately predict end-member discharges.

### *5.3 Terrain Analysis*

The observed trend in increased groundwater contribution with increased catchment scale implies that streamflow is a 3D integration of individual hillslope responses superimposed on larger-scale regional flow paths (**figure 16**). We attribute the increased importance of groundwater discharge to increased accumulated areas, and thereby available water for streamflow generation. These results suggest active inter-catchment groundwater flow. This finding is consistent with other regional scale studies (e.g. Tóth, 1963; Tóth, 1995; Frisbee *et al.*, 2011). In this study, we utilize multiple lines of evidence to show this relationship at a landscape scale that is orders of magnitude smaller than what previous research has observed. The relationship was generally consistent across variable streamflow states but small temporal inconsistencies are likely associated with dynamic catchment properties like climate and soil moisture, highlighting the importance of antecedent conditions.

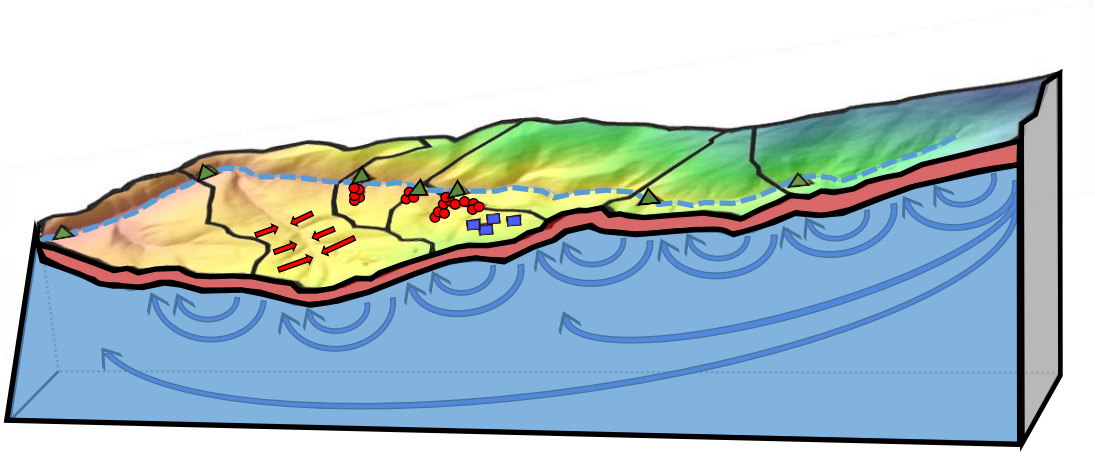

*Figure 16. A 3D conceptual model of CWW showing that the creek is an integration of regional groundwater flowpaths that contribute to streamflow at lower elevations as well individual hillslope responses.*

In addition, we observed a relationship between elevation and groundwater discharge where lower elevations correspond to increased proportions of groundwater in streamflow generation, exposing the importance of topography in the hydraulics of catchment-scale transport. Together, these results indicate that internal landscape form (topography) as well as catchment scale are highly important to groundwater discharge. In addition, our methodology allows us to investigate the spatial scaling of this relationship, via the accumulated vs. incremental analysis.

The lack of structural trend in the incremental terrain index plots suggest that a minimum scale which is too small to observe trends in groundwater discharge with terrain metrics exists. The lack of trend at this scale could result from two proposed processes: 1) regional groundwater flow paths may contribute to streamflow in a non-linear fashion as they are focused by geologic heterogeneities, and 2) valley-bottom exchange of water. First, linear trends in modeled groundwater and soil water contributions against elevation and upslope accumulated area should not necessarily be expected at subscale as a sub-catchment high in the watershed with the same UAA as a sub-catchment lower in the watershed could export regional groundwater to locations lower in the watershed. Thus, in the case of active regional groundwater flow, low elevation sites would receive disproportionally more groundwater than high sites, which may give rise to the observed integrated correlations. Second, it is important to note that the chemical methods for analyzing incremental changes in discharge at each sub-catchment can only account for gains in streamflow. Thus, if significant valley bottom exchange occurs and water is lost to the hyporheic zone, any linear trends in discharge and landscape features would be disrupted as a result. When averaged over the whole catchment, however, local scale losses and gains are dampened as the catchment scale increases.

## 6. Conclusion

In this study, multiple environmental tracers and modeling techniques were used to understand the role that soil and deep bedrock groundwater have on streamflow generation along a 5 km reach of a snowmelt-dominated, mountainous catchment on spatial and temporal scales. $^{222}$Rn modeling indicates that streamflow is generated predominantly from subsurface sources both spatially and temporally. End-member mixing analysis results agreed, indicating that streamflow is driven by subsurface inflow, but was further able to partition streamflow into groundwater and soil water components. EMMA-derived mixing models show that headwaters are dominantly composed of soil water. The role of groundwater increases with increasing distance downstream. At the outlet, stream flow ranges from 26-44% groundwater with higher groundwater percentages observed during the wettest states of the catchment.

Mixing model results were compared with various landscape features in a 'cumulative' and 'incremental' sense to understand what features account for spatial heterogeneities in streamflow generation within the catchment. Cumulative analyses show elevation and upslope accumulated area to be first-order controls on groundwater discharge, highlighting the importance of internal catchment form and catchment area in relation to streamflow generation. As UAA increases and elevation decreases larger fractions of groundwater discharge were observed, suggesting topography-driven groundwater flow. Incremental analysis results suggest a scale threshold for landscape influence on end-member contributions.

The results of this study shed light on some of the fundamental processes controlling stream flow generation spatially and temporally.

- Groundwater discharge remains an important source of streamflow generation, throughout the year even in upland, snowmelt dominated catchments.
- Groundwater discharge responds rapidly to precipitation inputs

- Terrain accurately predicts the fraction of soil and groundwater contribution to streamflow at scales greater than individual hillslopes.
- A minimum threshold scale for which terrain does not predict groundwater fraction exists, and is of the order of individual hillslopes.

The results of this study imply that groundwater must be considered a significant source of storage and discharge even in upland, first-order catchments. The volume of groundwater circulation and storage will significantly affect catchment response to disturbance and climatic fluctuations.

## References


Amoozegar, A. 1989. A Compact Constant-Head Permeameter for Measuring Saturated Hydraulic Conductivity of the Vadose Zone. Soil Sci. Soc. Am. J. 53:1356-1361. doi:10.2136/sssaj1989.03615995005300050009x

Anderson, John, "Geochemical Assessment and Separation of Source Waters in the Upper Boulder River Watershed Near Boulder, MT" (2015). Graduate Theses & Non- Theses. 17.

Anderson, S. P., W. E. Dietrich, R. Torres, D. R. Montgomery, and K. Loague (1997), Concentration-discharge relationships in runoff from a steep, unchanneled catchment, *Water Resour. Res.*, 33(1), 211–225, doi: 10.1029/96WR02715.

Barnett, T.P., Adam, J.C., and Lettenmaier, D.P., 2005, Potential impacts of a warming climate on water availability in snow-dominated regions: Nature, v. 438, p. 303-309, doi: 10.1038/nature04141.

Brenner, R. L., (1968). The Geology of Lubrecht Experimental Forest, University of Montana Library, 1-77.

Briar, D.W et al. (1996), Ground-water levels in intermontane basins of the Northern Rocky Mountains, Montana and Idaho, *Hydrologic Investigations Atlas* HA-738-B, 1.

Brisette, Christine M., "Stream restoration effects on hydraulic exchange, storage and alluvial aquifer discharge" (2017). *Graduate Student Theses, Dissertations, and Professional Papers. 10992.*

Carey, S.K., and Quinton, W.L., 2005, Evaluating runoff generation during summer using hydrometric, stable isotope and hydrochemical methods in a discontinuous permafrost alpine catchment: Hydrological Processes, v. 19, p. 95-114, doi: 10.1002/hyp.5764.

Cayan, D.R., Kammerdiener, S.A., Dettinger, M.D., Caprio, J.M., and Peterson, D.H., 2001, Changes in the Onset of Spring in the Western United States: Bulletin of the American Meteorological Society, v. 82, p. 399-415, doi: CITOOS>2.3.CO;2.

Christophersen, N., Neal, C., Hooper, R.P., Vogt, R.D., and Andersen, S., 1990, Modelling streamwater chemistry as a mixture of soilwater end-members — A step towards second-

generation acidification models: Journal of Hydrology, v. 116, p. 307-320, doi: 10.1016/0022-1694(90)90130-P.

Clark, Emily N., (2015). "Quantifying the Spatio-temporal Variability of Subsurface Flow Across Three Hillslopes in a Semi-arid, Alpine Forest. Professional Paper University of Montana Library, 1-53.

Cook, P.G. et al., 2003. Determining natural groundwater influx to a tropical river using radon, chlorofluorocarbons and ionic environmental tracers. *Journal of Hydrology*, 277(1–2), pp.74–88.

Cook, P.G. et al., 2006. Quantifying groundwater discharge to Cockburn River, southeastern Australia, using dissolved gas tracers 222Rn and SF6. *Water Resources Research*, 42(10), pp.1–12.

Dewalle, D.R., Swistock, B.R., and Sharpe, W.E., 1988, Three-component tracer model for stormflow on a small Appalachian forested catchment: Journal of Hydrology, v. 104, p. 301-310, doi: 10.1016/0022-1694(88)90171-0.

Dunne, T. and Black, R.D. 1970: Partial area contributions to storm runoff in a small New England watershed. Water Resources Research 6, 1296–311.

Ellins, K.K., Roman-Mas, A., and Lee, R., 1990, Using 222Rn to examine groundwater/surface discharge interaction in the Rio Grande de Manati, Puerto Rico: Journal of Hydrology, v. 115, p. 319-341, doi: 10.1016/0022-1694(90)90212-G.

Freeze, R. A. (1972a), Role of subsurface flow in generating surface runoff: 1. Base flow contributions to channel flow, *Water Resour. Res.*, 8(3), 609–623, doi: 10.1029/WR008i003p00609.

Frisbee, M. D., F. M. Phillips, A. R. Campbell, F. Liu, and S. A. Sanchez (2011), Streamflow generation in a large, alpine watershed in the southern Rocky Mountains of Colorado: Is streamflow generation simply the aggregation of hillslope runoff responses?, *Water Resour. Res.*, 47, W06512, doi:10.1029/2010WR009391.

Frisbee M. D., Phillips F. M., Weissmann G. S., Brooks P. D., Wilson J. L., Campbell A. R., and Liu F. (2012): Unraveling the mysteries of the large watershed black box: Implications for the streamflow response to climate and landscape perturbations. *Geophysical Research Letters 39: L01404*. DOI: 10.1029/2011GL050416

Fritz, P., Drimmie, R.J., & Render, F.W. (1974). *Stable isotope contents of a major prairie aquifer in Central Manitoba, Canada*. International Atomic Energy Agency (IAEA): IAEA.

Gardner, W.P., Harrington, G.A., Solomon, D.K., and Cook, P.G., 2011, Using terrigenic 4He to identify and quantify regional groundwater discharge to streams: Water Resources Research, v. 47, , doi: 10.1029/2010WR010276.

Genereux, D.P., and Hemond, H.F., 1990, Naturally Occurring Radon 222 as a Tracer for Streamflow Generation: Steady State Methodology and Field Example: Water Resources Research, v. 26, p. 3065-3075, doi: 10.1029/WR026i012p03065.

Genereux, D.P., Hemond, H.F., and Mulholland, P.J., 1993, Use of radon-222 and calcium as tracers in a three-end-member mixing model for streamflow generation on the West Fork of Walker Branch Watershed: Journal of Hydrology, v. 142, p. 167-211, doi: 10.1016/0022-1694(93)90010-7.

Goldich, S.S., 1938, A Study in Rock-Weathering: The Journal of Geology, v. 46, p. 17-58, doi: 10.1086/624619.

Grayson, R.B., Western, A.W., Chiew, F.H.S., and Blöschl, G., 1997, Preferred states in spatial soil moisture patterns: Local and nonlocal controls: Water Resources Research, v. 33, p. 2897-2908, doi: 10.1029/97WR02174.

Hale, V.C., and McDonnell, J.J., 2016, Effect of bedrock permeability on stream base flow mean transit time scaling relations: 1. A multiscale catchment intercomparison: Water Resources Research, v. 52, p. 1358-1374, doi: 10.1002/2014WR016124.

Herrmann, A., and Stichler, W., 1980, Groundwater-Runoff relationships: Catena, v. 7, p. 251-263, doi: 10.1016/S0341-8162(80)80017-8.

Hewlett, J.D. and Hibbert, A.R. (1967) Factors Affecting the Response of Small Watersheds to Precipitation in Humid Areas. In: Sopper, W.E. and Lull, H.W., Eds., Proceedings of the International Symposium on Forest Hydrology, Pergamon, Pennsylvania State University, New York, 275-290.

Hooper, R.P., and C.A. Shoemaker (1986), A comparison of chemical and isotopic hydrograph separation. Water Resource Research 22, 1444-1454.

Holden, Z. A., J. T. Abatzoglou, C. H. Luce, and L. S. Baggett (2011), Empirical downscaling of daily minimum air temperature at very fine resolutions in complex terrain, *Agric. For. Meteorol.*, *151*(8), 1066–1073, doi:10.1016/j.agrformet.2011.03.011.

Holden, Z. A., M. A. Crimmins, S. A. Cushman, and J. S. Littell (2011a), Empirical modeling of spatial and temporal variation in warm season nocturnal air temperatures in two North Idaho mountain ranges, USA, *Agric. For. Meteorol.*, *151*(3), 261–269, doi:10.1016/j.agrformet.2010.10.006.

Horton, R.E., 1933, The Rôle of infiltration in the hydrologic cycle: Eos, Transactions American Geophysical Union, v. 14, p. 446-460, doi: 10.1029/TR014i001p00446.

Hoylman, Z. H., Jencso, K. G., Hu, J., Holden, Z. A., Martin, J. T., (in review). Hydrology across the critical zone: Topography and climate control the spatial and temporal organization of vapor pressure deficit, soil moisture and shallow subsurface flow. Water Resources Research.

Hvorslev, M.J., 1951. Time Lag and Soil Permeability in Ground-Water Observations, Bull. No. 36, Waterways Exper. Sta. Corps of Engrs, U.S. Army, Vicksburg, Mississippi, pp. 1-50

Jencso, K.G., McGlynn, B.L., Gooseff, M.N., Wondzell, S.M., Bencala, K.E., and Marshall, L.A., 2009, Hydrologic connectivity between landscapes and streams: Transferring reach- and plot-scale understanding to the catchment scale: Water Resources Research, v. 45, p. n/a, doi: 10.1029/2008WR007225.

Kienzler, P.M., and Naef, F., 2008, Subsurface storm flow formation at different hillslopes and implications for the 'old water paradox': Hydrological Processes, v. 22, p. 104-116, doi: 10.1002/hyp.6687.

Kies, A., Hofmann, H., Tosheva, Z., Hoffmann, L., Pfister,L., 2005, Using 222 Rn for hydrograph separationin a micro basin (Luxembourg): Annals of Geophysics, v. 48, , doi: 10.4401/ag-3184.

Kennedy, V.C., Kendall, C., Zellweger, G.W., Wyerman, T.A., and Avanzino, R.J., 1986, Determination of the components of stormflow using water chemistry and environmental isotopes, Mattole River basin, California: Journal of Hydrology, v. 84, p. 107-140, doi: 10.1016/0022-1694(86)90047-8.

Klaus, J., and McDonnell, J.J., 2013, Hydrograph separation using stable isotopes: Review and evaluation: Journal of Hydrology, v. 505, p. 47-64, doi: 10.1016/j.jhydrol.2013.09.006.

Landon, M.K., Delin, G.N., Komor, S.C., and Regan, C.P., 1999, Comparison of the stable-isotopic composition of soil water collected from suction lysimeters, wick samplers, and cores in a sandy unsaturated zone: Journal of Hydrology, v. 224, p. 45-54.

Lee, R.W., and Hollyday, E.F., April 7-9, 1987, Radon Measurement in Streams to Determine Location and Magnitude of Ground-Water Seepage.

Lonn, J.D., McDonald, C., Sears, J.W., Smith, L.N., 2010, Geologic Map of the Missoula East 30' x 60' Quadrangle, Western Montana. MBMG Open File Report 593.

McDonnell, J.J., M.K. Stewart and I.F. Owens (1991). Effects of catchment-scale subsurface watershed mixing on stream isotopic response. Water Resources Research, 27(12): 3065-3073.

McDonnell, J.J., 2014, The two water worlds hypothesis: ecohydrological separation of water between streams and trees? Wiley Interdisciplinary Reviews: Water, v. 1, p. 323-329, doi: 10.1002/wat2.1027.

McGuire, K.J., McDonnell, J.J., Weiler, M., Kendall, C., McGlynn, B.L., Welker, J.M., Seibert, J., 2005, The role of topography on catchment-scale water residence time: Water Resources Research, v. 41, p. n/a, doi: 10.1029/2004WR003657.

Messerli, B., D. Viviroli, and R. Weingartner (2004), Mountains of the world: Vulnerable water towers for the 21st century, Ambio Spec. Rep., 13, 29–34.

Mote, P.W., Hamlet, A.F., Clark M.P., Lettenmaier, D.P., 2005, DECLINING MOUNTAIN SNOWPACK IN WESTERN NORTH AMERICA: Bulletin of the American Meteorological Society, v. 86, p. 39-49, doi: 10.1175/BAMS-86-1-39.

National Cooperative Soil Survey. National Cooperative Soil Characterization Database. Available online. Accessed [04/26/2018].

Negulescu, M., and Rojanski, V., 1969, Recent research to determine reaeration coefficient: Water Research, v. 3, p. 192,IN6,202, doi: 10.1016/0043-1354(69)90058-X.

O'Connor, D.J., Dobbins, W.E., 1958. Mechanism of reaeration in natural streams. Trans. Am. Soc. Civ. Engrs, 123 (2934) (1958), p. 641

Pfister, L., Martínez-Carreras, N., Hissler, C., Klaus, J., Carrer, G.E., Stewart, M.K., and McDonnell, J.J., 2017, Bedrock geology controls on catchment storage, mixing, and release: A comparative analysis of 16 nested catchments: Hydrological Processes, v. 31, p. 1828-1845, doi: 10.1002/hyp.11134.

Pinder, G. F., and J. F. Jones (1969), Determination of the ground-water component of peak discharge from the chemistry of total runoff, Water Resour. Res., 5(2), 438–445, doi:10.1029/WR005i002p00438

Portner, R.A., Hendrix, M.S., Stalker, J.C., Miggins, D.P., and Sheriff, S.D., 2011, Sedimentary response to orogenic exhumation in the northern Rocky Mountain Basin and Range province, Flint Creek basin, west-central Montana: Canadian Journal of Earth Sciences, v. 48, p. 1131-1154, doi: 10.1139/e10-107.

Raymond, P.A., Zappa, C.J., Butman, D., Bott, T.L., Potter, J., Mulholland, P., Laursen, A.E., McDowell, W.H., and Newbold, D., 2012, Scaling the gas transfer velocity and hydraulic geometry in streams and small rivers: Limnology and Oceanography: Fluids and Environments, v. 2, p. 41-53, doi: 10.1215/21573689-1597669.

Rogers, A.S., 1958, Physical behavior and geologic control of radon in mountain streams [Utah]: U.S. Geological Survey Bulletin, p. 187-211.

Sklash, M.G., R.N. Farvolden, and P. Fritz. 1976. A conceptual model of watershed response to rainfall, developed through the use of oxygen-18 as a natural tracer. Canadian Journal of Earth Science 13, 271-283.

Sklash, M.G., and R.N. Farvolden. 1979. The role of groundwater in storm runoff. Journal of Hydrology 43, 45- 65.

Stephenson, D.A., 1980, Contemporary Hydrogeology : The George Burke Maxey memorial volume: Netherlands, Elsevier Science.

Swistock, B.R., DeWalle, D.R., and Sharpe, W.E., 1989, Sources of acidic storm flow in an Appalachian Headwater Stream: Water Resources Research, v. 25, p. 2139-2147, doi: 10.1029/WR025i010p02139.

Tague, C., and G. E. Grant (2009), Groundwater dynamics mediate low-flow response to global warming in snow-dominated alpine regions, *Water Resour. Res.*, 45, W07421, doi: 10.1029/2008WR007179.

Thornthwaite, C.W. (1961) THE TASK AHEAD, Annals of the Association of American Geographers, 51:4,345-356, DOI: 10.1111/j.1467-8306.1961.tb00385.x

Tóth, J. (1963), A theoretical analysis of groundwater flow in small drainage basins, *J. Geophys. Res.*, 68(16), 4795–4812, doi:10.1029/JZ068i016p04795.

Tóth, J. (1995), Hydraulic continuity in large sedimentary basins, *Hydrogeol. J.*, **3**, 4–16.

## Appendix

*Table 1-A. Details solute concentrations used in EMMA mass-balance mixing models.*

| ***Tracer Concentration*** (mg/L) | ***Groundwater*** | ***Soil Water*** |
|---|---|---|
| Calcium | 7.94 | 2.72 |
| Chloride | 1.22 | 1.30 |
| Magnesium | 3.93 | 1.84 |
| Sodium | 8.47 | 2.39 |

*Table 2-A. Eigenvalues extracted from the EMMA covariance matrix with corresponding percentages of variance explained by each value. The last column tallies the cumulative variance explained by each consecutive eigenvalue.*

| ***PCA Component*** | ***Eigenvalue*** | ***% Var. Explained*** | ***Cumulative Var.*** |
|---|---|---|---|
| 1 | 5.370 | 59.67 | 59.67% |
| 2 | 1.858 | 20.65 | 80.32% |
| 3 | 0.866 | 9.62 | 89.94% |
| 4 | 0.363 | 4.04 | 93.98% |
| 5 | 0.260 | 2.89 | 96.87% |
| 6 | 0.150 | 1.67 | 98.54% |
| 7 | 0.107 | 1.18 | 99.72% |
| 8 | 0.018 | 0.20 | 99.92% |
| 9 | 0.007 | 0.08 | 100% |

*Table 3-A. Discharge, $^{222}Rn$ and major ion concentrations, and field parameters from synoptic sampling campaigns. Well locations are in UTM Zone 12N.*

| | Date & Time | Q (L/s) | $^{222}Rn$ Conc. (Bq/L) | Ca (mg/L) | K (mg/L) | Mg (mg/L) | Na (mg/L) | F (mg/L) | Cl (mg/L) | $SO_4$ (mg/L) | $NO_3$ (mg/L) | Temp. (°C) | pH | ORP (mV) | Spec. Cond. (µS/cm) |
|---|---|---|---|---|---|---|---|---|---|---|---|---|---|---|---|
| CWSTW1 *12N 318545.9409 E, 5196211.4225 N* | 03/31/2017 10:01 AM | 11.84 | 0.659 | 5.923 | 2.988 | 3.126 | 6.821 | 0.1558 | 4.6771 | 1.1959 | 2.4762 | 3.5 | 7.9 | - | 65.1 |
| | 04/28/2017 9:35 AM | 9.98 | 0.111 | 5.085 | 2.451 | 2.730 | 5.188 | 0.0951 | 3.1206 | 1.6835 | 0.6937 | 4.0 | 8.4 | 74.3 | 69.4 |
| | 05/12/2017 8:51 AM | 7.72 | 0.174 | 5.513 | 2.668 | 2.964 | 5.335 | 0.0964 | 3.0017 | 1.5636 | 0.4802 | 7.6 | 8.9 | -15.0 | 41.2 |
| | 5/19/2017 8:49 AM | 12.50 | - | 5.064 | 2.374 | 2.653 | 4.812 | 0.1069 | 2.9297 | 1.4078 | 0.5095 | 4.2 | 9.0 | -92.4 | 37.7 |
| | 06/02/2017 11:53 AM | 11.50 | 0.184 | 5.626 | 2.512 | 3.09 | 5.694 | 0.0844 | 1.6343 | 1.3527 | 0.5394 | 9.0 | 9.2 | -42.8 | 41.4 |
| | 06/8/2017 13:14 PM | 9.18 | 0.210 | - | - | - | - | - | - | - | - | 10.9 | 9.0 | -46.2 | 42.9 |
| | 06/15/2017 12:46 PM | 21.76 | - | - | - | - | - | - | - | - | - | 8.6 | 8.3 | -19.0 | 52.9 |
| | 06/20/2017 9:08 AM | 16.67 | - | 5.644 | 2.489 | 2.956 | 5.629 | 0.0934 | 1.7774 | 1.3272 | 0.4358 | 9.6 | 7.9 | 64.9 | 44.0 |
| | 07/06/2017 7:39 AM | 8.81 | 0.110 | 5.513 | 2.537 | 2.997 | 5.512 | 0.0831 | 1.706 | 1.2803 | 0.3429 | 10.8 | 8.1 | 106.7 | 40.0 |
| | 07/24/2017 10:36 AM | 4.84 | 0.132 | 5.061 | 2.71 | 2.83 | 5.277 | 0.0969 | 1.5662 | 1.2922 | 0.4325 | 12.11 | 8.4 | 87.5 | 55.5 |
| | 9/28/2017 9:35 AM | - | 0.096 | 4.789 | 2.867 | 2.591 | 5.36 | 0.0699 | 1.4561 | 5.3113 | 0 | - | - | 143.9 | 73.2 |
| | 10/07/2017 10:44 AM | 3.11 | 0.458 | 5.031 | 3.147 | 2.657 | 5.604 | 0.0862 | 2.1656 | 6.8158 | 0.0318 | 7.95 | 5.4 | 70.3 | 70.3 |
| CWSTW2 (lower) *12N 319399.5898E, 5196641.9186N* | 03/31/2017 11:00 AM | 11.12 | 1.230 | 6.043 | 2.829 | 3.168 | 6.277 | 0.12 | 2.3329 | 2.0357 | 0.6058 | 3.6 | 7.1 | - | 65.3 |
| | 04/28/2017 10:39 AM | 9.08 | 0.984 | 5.304 | 2.473 | 2.845 | 5.233 | 0.1007 | 3.0785 | 1.5703 | 0.6154 | 4.38 | 8.6 | 53.7 | 67.2 |
| | 05/12/2017 9:25 AM | 6.98 | 0.348 | 5.25 | 2.64 | 2.871 | 5.1 | 0.0879 | 2.9244 | 1.4132 | 0.5871 | 7.2 | 9.7 | -61.4 | 39.8 |
| | 5/19/2017 9:38 AM | 11.67 | - | 5.159 | 2.373 | 2.703 | 4.73 | 0.0921 | 2.8034 | 1.2888 | 0.5243 | 4.2 | 9.4 | -69.1 | 36.6 |
| | 06/02/2017 12:32 PM | 10.76 | 0.615 | 5.39 | 2.406 | 2.96 | 5.438 | 0.0828 | 1.7058 | 1.3102 | 0.3549 | 9.1 | 9.3 | -32.6 | 28.2 |
| | 06/8/2017 13:49 PM | 8.20 | 0.317 | - | - | - | - | - | - | - | - | 10.3 | 9.2 | -55.2 | 42.5 |
| | 06/15/2017 13:35 PM | 18.85 | - | - | - | - | - | - | - | - | - | 8.2 | 8.3 | -21.5 | 52.4 |

| | | | | | | | | | | | | | | | |
|---|---|---|---|---|---|---|---|---|---|---|---|---|---|---|---|
| | 06/20/2017 9:39 AM | 15.72 | - | 5.613 | 2.5 | 3.016 | 5.589 | 0.0879 | 1.689 | 1.2762 | 0.4409 | 9.0 | 8.7 | 64.9 | 44.0 |
| | 07/06/2017 8:15 AM | 7.98 | 0.514 | 5.347 | 2.485 | 2.938 | 5.324 | 0.0834 | 1.6929 | 1.2335 | 0.419 | 10.0 | 9.1 | 106.7 | 40.1 |
| | 07/24/2017 11:19 AM | 5.02 | 0.140 | 4.749 | 2.708 | 2.63 | 4.878 | 0.0767 | 1.6068 | 1.1042 | 0.4456 | 12.3 | 8.1 | 34.2 | 51.6 |
| | 9/28/2017 10:26 AM | - | 0.578 | 4.543 | 2.869 | 2.429 | 4.706 | 0.0787 | 1.7271 | 6.7063 | 0.0336 | 6.19 | 6.3 | 124.5 | 70.8 |
| | 10/07/2017 11:45 AM | 3.49 | 0.890 | 4.61 | 2.965 | 2.401 | 4.936 | 0.0686 | 2.3471 | 5.405 | 0.0297 | 7.8 | 6.9 | 39.0 | 74.9 |
| CWSTW2 (upper) *12N 320274.3732E, 5196302.233N* | 03/31/2017 12:03 PM | 7.84 | 0.925 | 5.381 | 2.53 | 2.986 | 5.297 | 0.1288 | 1.9205 | 1.4798 | 0.5848 | 3.4 | 7.9 | 105.5 | 58.1 |
| | 04/28/2017 11:25 AM | 7.76 | 0.625 | 4.635 | 2.299 | 2.64 | 4.617 | 0.0762 | 2.7887 | 1.1344 | 0.6541 | 4.7 | 9.8 | -40.0 | 58.6 |
| | 05/12/2017 10:28 AM | 6.20 | 0.564 | - | - | - | - | - | - | - | - | 7.7 | 9.5 | -60.5 | 35.0 |
| | 5/19/2017 10:45 AM | 11.36 | - | 4.757 | 2.271 | 2.623 | 4.516 | 0.1003 | 2.7955 | 0.9965 | 0.5002 | 5.3 | 9.8 | -57.7 | 33.0 |
| | 06/02/2017 13:13 PM | 9.01 | 0.513 | 4.797 | 2.199 | 2.74 | 4.777 | 0.0702 | 1.3157 | 0.9106 | 0.4256 | 9.5 | 9.1 | -45.1 | 24.9 |
| | 06/8/2017 14:41 PM | 6.82 | 0.263 | - | - | - | - | - | - | - | - | 10.3 | 8.9 | -79.0 | 36.6 |
| | 06/15/2017 14:11 PM | 17.55 | - | - | - | - | - | - | - | - | - | 8.4 | 8.0 | -11.2 | 45.3 |
| | 06/20/2017 10:31 AM | 13.64 | - | 5.086 | 2.219 | 2.79 | 4.893 | 0.0819 | 1.4924 | 0.9732 | 0.4177 | 9.3 | 8.7 | -23.8 | 38.9 |
| | 07/06/2017 8:52 AM | 6.63 | 0.257 | 4.711 | 2.299 | 2.681 | 4.642 | 0.078 | 1.3801 | 0.8776 | 0.3329 | 10.1 | 8.8 | 19.2 | 34.3 |
| | 07/24/2017 12:14 PM | 4.33 | 0.233 | 4.154 | 2.439 | 2.333 | 4.074 | 0.0669 | 1.2328 | 0.8163 | 0.4403 | 12.0 | 7.7 | 6.9 | 45.5 |
| | 10/07/2017 12:35 PM | 3.34 | 0.608 | 4.264 | 2.908 | 2.278 | 4.244 | 0.0064 | 0.1549 | 0.3276 | 0 | 8.2 | 5.6 | 89.4 | 71.8 |
| CWSTW6 *12 N 320735.994E, 5196074.7036N* | 03/31/2017 13:10 PM | 6.96 | 4.640 | 5.176 | 2.26 | 2.894 | 5.155 | 0.1172 | 1.8292 | 1.315 | 0.6672 | 2.9 | 8.0 | 87.3 | 57.4 |
| | 04/28/2017 12:26 PM | 7.42 | 4.249 | 4.256 | 2.01 | 2.441 | 4.383 | 0.0758 | 3.0039 | 1.0263 | 0.6072 | 4.3 | 9.4 | -70.0 | 56.8 |
| | 05/12/2017 11:10 AM | 5.45 | 3.188 | 4.388 | 2.273 | 2.527 | 4.218 | 0.0788 | 2.7045 | 0.9479 | 0.5918 | 7.3 | 8.8 | -42.9 | 34.2 |
| | 5/19/2017 11:24 AM | 10.98 | - | 4.758 | 2.15 | 2.686 | 4.416 | 0.0876 | 2.6566 | 0.8982 | 0.5028 | 5.0 | 9.1 | -52.4 | 33.3 |
| | 06/02/2017 13:53 PM | 8.18 | 3.364 | 4.611 | 2.09 | 2.675 | 4.596 | 0.0679 | 1.2267 | 0.8486 | 0.4709 | 8.9 | 9.0 | -54.2 | 34.4 |
| | 06/9/2017 10:25 AM | 6.28 | 2.269 | - | - | - | - | - | - | - | - | 8.9 | 8.9 | -39.6 | 35.2 |

| | | | | | | | | | | | | | | | |
|---|---|---|---|---|---|---|---|---|---|---|---|---|---|---|---|
| | 06/15/2017 15:17 PM | 17.08 | - | - | - | - | - | - | - | - | - | 7.9 | 8.3 | -24.0 | 46.1 |
| | 06/20/2017 11:10 AM | 13.39 | - | 4.836 | 2.082 | 2.716 | 4.802 | 0.0754 | 1.4954 | 0.9223 | 0.4774 | 9.1 | 7.8 | 27.7 | 37.9 |
| | 07/06/2017 9:49 AM | 6.19 | 2.210 | 4.44 | 2.104 | 2.566 | 4.309 | 0.0684 | 1.3764 | 0.8181 | 0.3963 | 10.5 | 8.6 | 13.8 | 32.8 |
| | 07/24/2017 13:39 PM | 3.39 | 2.685 | 3.865 | 2.255 | 2.189 | 3.801 | 0.0627 | 1.3338 | 0.7606 | 0.5409 | 12.0 | 7.2 | 11.0 | 43.1 |
| | 10/07/2017 13:37 PM | 3.05 | 2.437 | 4.071 | 2.676 | 2.218 | 3.915 | 0.0566 | 1.8054 | 3.7685 | 0.0317 | 7.7 | 6.7 | 46.4 | 71.7 |
| CWSTW7 *12N 320836.6154E, 5196046.8234N* | 03/31/2017 13:30 PM | 4.46 | 1.120 | 4.238 | 2.106 | 2.451 | 4.052 | 0.1473 | 1.5519 | 1.071 | 0.6149 | 2.6 | 7.5 | 114.5 | 47.9 |
| | 04/28/2017 12:58 PM | 5.56 | 1.979 | 3.602 | 1.941 | 2.15 | 3.485 | 0.0632 | 2.5544 | 0.8023 | 0.5546 | 3.9 | 9.1 | -51.9 | 48.0 |
| | 05/12/2017 11:46 AM | 4.12 | 0.698 | 3.842 | 2.172 | 2.272 | 3.624 | 0.0671 | 2.3568 | 0.7742 | 0.423 | 7.2 | 9.0 | -45.3 | 29.5 |
| | 5/19/2017 11:50 AM | 9.21 | - | 4.066 | 1.972 | 2.31 | 3.714 | 0.0673 | 2.4044 | 0.7161 | 0.4458 | 4.4 | 9.0 | -35.3 | 15.5 |
| | 06/02/2017 14:26 PM | 6.17 | 0.833 | 3.737 | 1.855 | 2.243 | 3.675 | 0.0613 | 1.1523 | 0.651 | 0.4034 | 8.9 | 9.0 | -54.2 | 34.4 |
| | 06/9/2017 10:53 AM | 4.91 | 0.732 | - | - | - | - | - | - | - | - | 9.1 | 9.3 | -61.8 | 30.0 |
| | 06/15/2017 15:41 PM | 14.06 | - | - | - | - | - | - | - | - | - | 8.0 | 7.4 | 32.4 | 40.4 |
| | 06/20/2017 11:33 AM | 10.41 | - | 4.135 | 1.893 | 2.368 | 4.023 | 0.074 | 1.3058 | 0.7486 | 0.4195 | 8.8 | 8.3 | 6.6 | 32.7 |
| | 07/06/2017 10:20 AM | 4.50 | 0.643 | 4.014 | 2.01 | 2.381 | 3.931 | 0.0614 | 1.3025 | 0.6983 | 0.4505 | 10.2 | 8.3 | 49.8 | 29.6 |
| | 07/24/2017 14:13 PM | 2.67 | 0.664 | 3.726 | 2.142 | 2.155 | 3.631 | 0.0572 | 1.0992 | 0.6657 | 0.4135 | 11.2 | 8.2 | -13.7 | 40.8 |
| | 10/07/2017 14:14 PM | 2.15 | 0.564 | 3.76 | 2.635 | 2.123 | 3.517 | 0.0463 | 1.8551 | 3.2883 | 0.03 | 7.1 | 6.3 | 43.4 | 70.8 |
| CWSTW8 *12N 321955.3742E, 5195586.0398N* | 03/31/2017 14:45 PM | 2.43 | 0.702 | 3.768 | 1.785 | 2.581 | 3.364 | 0.0432 | 1.3664 | 0.8115 | 0.512 | 1.6 | 8.3 | 74.0 | 42.0 |
| | 04/28/2017 14:23 PM | 3.89 | 0.539 | - | - | - | - | - | - | - | - | 3.7 | 9.0 | -65.0 | 39.1 |
| | 05/19/2017 13:46 PM | 8.27 | - | 3.432 | 1.71 | 2.334 | 3.196 | 0.0509 | 1.0751 | 0.5438 | 0.4132 | 4.8 | 10.0 | -86.6 | 24.7 |
| | 06/02/2017 15:19 PM | 4.33 | 0.262 | 2.879 | 1.54 | 2.049 | 2.868 | 0.05 | 0.8474 | 0.481 | 0.3859 | 9.3 | 9.1 | -53.0 | 23.0 |
| | 06/9/2017 12:03 PM | 3.23 | 0.105 | - | - | - | - | - | - | - | - | 9.2 | 8.9 | -44.8 | 23.6 |
| | 06/15/2017 16:27 PM | 9.74 | - | - | - | - | - | - | - | - | - | 7.9 | 7.9 | -13.5 | 34.9 |

| | | | | | | | | | | | | | | | |
|---|---|---|---|---|---|---|---|---|---|---|---|---|---|---|---|
| | 06/20/2017 12:36 PM | 6.81 | - | 3.142 | 1.548 | 2.167 | 3.211 | 0.0546 | 1.1074 | 0.6053 | 0.4295 | 9.5 | 8.2 | -4.9 | 26.6 |
| | 07/24/2017 15:00 PM | 1.46 | 0.195 | 2.761 | 1.634 | 1.883 | 2.473 | 0 | 0.2404 | 0.0859 | 0 | 12.4 | 8.0 | 46.6 | 30.2 |
| | 10/07/2017 14:14 PM | 1.32 | 0.255 | 2.912 | 2.266 | 1.741 | 2.246 | 0.0328 | 1.6387 | 2.136 | 0.1104 | 6.9 | 5.9 | 47.7 | 65.1 |
| CWSTW9 *12N 322850.9823E, 5195581.893 N* | 03/31/2017 15:30 PM | 2.21 | 0.530 | 3.381 | 1.807 | 2.26 | 3.01 | 0.0659 | 1.0586 | 0.6181 | 0 | 1.9 | 7.8 | 91.1 | 37.1 |
| | 04/28/2017 15:25 PM | 3.46 | 0.402 | 2.752 | 1.62 | 1.945 | 2.547 | 0.0681 | 2.1954 | 0.4879 | 0.6007 | 4.1 | 9.1 | -61.5 | 34.2 |
| | 05/12/2017 12:50 PM | 2.74 | 0.604 | 2.457 | 1.695 | 1.724 | 2.24 | 0.0432 | 2.0405 | 0.3862 | 0.4366 | 8.0 | 8.9 | 48.9 | 20.8 |
| | 5/19/2017 14:37 PM | 7.08 | - | 3.185 | 1.687 | 2.142 | 2.965 | 0.0571 | 2.1465 | 0.4767 | 0.478 | 4.9 | 9.0 | -64.0 | 23.4 |
| | 06/02/2017 16:10 PM | 3.33 | 0.314 | 2.565 | 1.507 | 1.806 | 2.472 | 0.0472 | 0.5799 | 0.3235 | 0.3745 | 9.0 | 8.9 | -53.0 | 20.5 |
| | 06/9/2017 12:49 PM | 3.30 | 0.469 | - | - | - | - | - | - | - | - | 9.0 | 8.5 | -33.0 | 21.4 |
| | 06/15/2017 17:18 PM | 6.64 | - | - | - | - | - | - | - | - | - | 8.0 | 7.7 | 3.1 | 32.5 |
| | 06/20/2017 13:14 PM | 6.69 | - | 2.669 | 1.486 | 1.855 | 2.693 | 0 | 0.2326 | 0.0769 | 0 | 9.4 | 8.0 | 12.8 | 23.2 |
| | 07/06/2017 11:47 AM | 2.46 | 0.123 | 2.704 | 1.483 | 1.889 | 2.484 | 0.0473 | 0.7049 | 0.2904 | 0.379 | 10.9 | 8.7 | 20.0 | 20.6 |
| | 07/25/2017 8:42 AM | 2.04 | 0.177 | 2.686 | 1.97 | 1.675 | 2.116 | 0.0397 | 0.6894 | 1.000 | 0.0969 | 10.3 | - | - | 35.1 |
| | 09/28/2017 11:58 AM | - | 0.310 | 2.493 | 1.961 | 1.616 | 1.817 | 0.0347 | 0.7963 | 0.9474 | 0.0182 | 6.6 | 6.2 | 114.6 | 53.0 |
| | 10/07/2017 14:14 PM | 1.40 | 0.361 | 2.614 | 2.215 | 1.63 | 1.997 | 0.0295 | 1.7528 | 1.2563 | 0.0313 | - | - | - | - |
| CWUS GW Well *12N 321159.3127E, 5195626.4266N* | 04/07/2017 10:20 AM | - | 5.194 | 11.39 | 3.119 | 5.229 | 5.528 | 0.1459 | 2.069 | 1.9064 | 0.9752 | 5.0 | 7.9 | -22.3 | 94.4 |
| | 04/21/2017 14:50 PM | - | - | - | - | - | - | - | - | - | - | 6.3 | 6.5 | 6.2 | 114.0 |

| | | | | | | | | | | | | | | | |
|---|---|---|---|---|---|---|---|---|---|---|---|---|---|---|---|
| CWWH GW Well *12N 321190.4708E, 5195643.1938N* | 04/07/2017 11:46 AM | - | 1.531 | 18.67 | 3.276 | 3.457 | 6.994 | 0.0413 | 0.3387 | 0.1132 | 0.4324 | 7.7 | 8.7 | -52.9 | 110.3 |
| | 04/21/2017 15:10 PM | - | - | - | - | - | - | - | - | - | - | 7.5 | 7.9 | 41.3 | 142.5 |
| CWWH Soil Well *12N 321190.4708E, 5195643.1938N* | 04/07/2017 12:01 PM | - | 1.82 | 6.119 | 2.202 | 2.008 | 4.586 | 0.0042 | 0.2126 | 0.0411 | 0 | 6.9 | 6.5 | 25.7 | 43.8 |
| CWEH GW Well *12N 321191.5894E, 5195642.5767N* | 04/07/2017 13:00 PM | - | 4.750 | 38.66 | 6.094 | 5.17 | 12.05 | 0.2197 | 4.0709 | 2.9926 | 2.3979 | 7.7 | 7.5 | 60.4 | 132.4 |
| CWEH Soil Well *12N 321191.5894E, 5195642.5767N* | 04/07/2017 13:30 PM | - | 1.781 | 10.39 | 3.473 | 4.02 | 7.212 | 0.189 | 2.5741 | 1.5494 | 0.8925 | 7.7 | 5.6 | 98.7 | 87.4 |
| CWSW3 Soil Well *12N 320811.5936E, 5195938.9807N* | 04/21/2017 | - | 18.20 | - | - | - | - | - | - | - | - | 5.7 | 6.0 | 106.0 | 78.0 |

| | | | | | | | | | | | | | | | |
|---|---|---|---|---|---|---|---|---|---|---|---|---|---|---|---|
| CWSW5 Soil Well *12N 320795.1136E ,5195921.1934N* | 04/21/2017 | - | - | - | - | - | - | - | - | - | - | 5.6 | 6.6 | 68.0 | 78.0 |
| CWSW6 Soil Well *12N 320775.7738E, 5195884.6244* | 04/21/2017 | - | 3.916 | - | - | - | - | - | - | - | - | 6.3 | 6.7 | 27.0 | 81.3 |
| CWSW11 Soil Well *12N 320872.8792E, 5195852.7509N* | 04/21/2017 | - | - | - | - | - | - | - | - | - | - | 6.3 | 6.5 | 6.2 | 114.0 |
| CWSW12 Soil Well *12N 320960.2184E, 5195790.259N* | 04/21/2017 | - | 1.532 | - | - | - | - | - | - | - | - | 5.5 | 6.8 | -51.8 | 88.5 |
| Seep downslope from CWSW4 (soil well) | 04/21/2017 | | 19.310 | - | - | - | - | - | - | - | - | 5.2 | 6.7 | 78.0 | 78.0 |